1 **A consistent ocean oxygen profile dataset with new quality control and bias assessment**

3 Viktor Gourteski[1], Lijing Cheng[1], Juan Du[1], Xiaogang Xing[2], Fei Chai[3,4]

4 [1] Institute of Atmospheric Physics, Chinese Academy of Sciences, Beijing, China

5 [2] State Key Laboratory of Satellite Ocean Environment Dynamics, Second Institute of Oceanography, Ministry of

6 Natural Resources, Hangzhou, China

7 [3] State Key Laboratory of Marine Environmental Science, Xiamen University, Xiamen, China

8 [4] College of Ocean and Earth Sciences, Xiamen University, Xiamen, China

10 *Correspondence to*: Viktor Gouretski (viktor.gouretski@posteo.de);

11 Lijing Cheng (chenglij@mail.iap.ac.cn)

14 **Abstract.** The global ocean oxygen concentrations have declined in the past decades, posing threats to marine life and

15 human society. High-quality and bias-free observations are crucial to understanding the ocean oxygen changes and

16 assessing their impact. Here, we propose a new automated quality control (QC) procedure for ocean profile oxygen

17 data. This procedure consists of a suite of ten quality checks, with outlier rejection thresholds being defined based on

18 underlying statistics of the data. The procedure is applied to three main instrumentation types: bottle casts, CTD

19 (Conductivity-Temperature-Depth) casts, and Argo profiling floats. Application of the quality control procedure to

20 several manually quality-controlled datasets of good quality suggests the ability of the scheme to successfully identify

21 outliers in the data. Collocated quality-controlled oxygen profiles obtained by means of the Winkler titration method are

22 used as unbiased references to estimate possible residual biases in the oxygen sensor data. The residual bias is found to

23 be negligible for electrochemical sensors typically used on CTD casts. We explain this as the consequence of adjusting

24 to the concurrent sample Winkler data. Our analysis finds a prevailing negative residual bias for the delayed-mode

25 quality-controlled and adjusted profiles from Argo floats varying from -4 to -1 µmol kg^{-1} among the data subsets

26 adjusted by different Argo data assembly centers (DACs). The respective overall DAC-specific corrections are

27 suggested. Applying the new QC procedure and bias adjustment resulted in a new global ocean oxygen dataset from

28 1920 to 2023 with consistent data quality across bottle samples, CTD casts, and Argo floats. The adjusted Argo profile

29 data is available at the Marine Science Data Center of the Chinese Academy of Sciences (Gouretski et al., 2023,

30 http://dx.doi.org/10.12157/IOCAS.20231208.001)

1 Introduction

33   Progressive warming caused by the human-induced increase of the greenhouse gases in the Earth's atmosphere

34 leads to the decline of the dissolved oxygen concentration in the global ocean because of the reduction in oxygen

35 solubility, the increase in stratification, which hampers the exchange between the surface layer and the ocean interior,

36 and the accompanying change of ocean circulation (Keeling et al., 2010; Gruber et al., 2011; Deutsch et al., 2011;

37 Praetorius et al., 2015; Oschlies et al., 2018). Another factor related to human activities is the increasing input of

38 nutrients from agriculture and wastewater in the coastal regions (Oschlies et al., 2018; Breitburg et al., 2018). Nutrients

39   facilitate the growth of phytoplankton and microbes subsequently decrease oxygen levels after the phytoplankton dies

40   (Breitburg et al., 2018; Pitcher et al., 2021).

41   Recognizing the crucial role of dissolved oxygen for marine aerobic organisms, oceanographers started to measure

42   oxygen in the late 19th century using the chemical method developed by Winkler (1888). Since then, Winkler titration

43   has been a standard method used on oceanographic ships and in laboratories (Langdon, 2010), and the technique has an

44   accuracy estimated to be 0.1% or ±0.3 μmol kg^{-1} (Carpenter, 1965).

45   With the rapid technological progress during the 1960-70s and the development of the electronic CTD

46   (Conductivity-Temperature-Depth) profilers, the first electrochemical sensors appeared, providing the possibility for

47   continuous oxygen profiling, which is not possible with the Winkler method restricted by water samples from several

48   depth levels. Electrochemical sensors are based on a Clark polarographic membrane (Clark et al., 1953). Oxygen

49   concentration outside the membrane and oxygen diffusion through the membrane determine the sensor response.

50   Electrochemical Clark-type sensors possess a very fast time response (<1 s), with an initial accuracy of 2% of oxygen

51   saturation and precision of about 1 μmol kg^{-1} (Coppola et al., 2013). However, sensor drift AQC_FINAL_CTD.fdue to

52   membrane fouling and changes in electrolyte over time requires periodic calibration. The first type of sensors applied

53   on Biogeochemical Argo profiling floats (BGC floats) were Clark-type electrodes (Riser and Johnson, 2008).

54   Optical oxygen sensors called "optodes" are based on the principle of fluorescence quenching of a fluorescent

55   indicator embedded in a sensing foil (Körtzinger et al., 2005, Tengberg et al., 2006). The optode sensors appeared soon

56   after the first implementation of the Clark-type sensors on Argo floats (Gruber et al., 2010). Compared to

57   electrochemical sensors, optodes are characterized by long-term stability and high precision with the disadvantage of a

58   slower response time (Gregoire et al., 2021). During the initial period of several years, both Clarke-type and optode

59   sensors were used on Argo floats (Claustre et al., 2020). However, drift and initial calibration issues with

60   electrochemical sensors have led to the increased implementation of optodes on Argo floats (Claustre et al., 2020), for

61   which calibration using simultaneous water samples is not possible. From the beginning of the BGC-Argo float

62   implementation until March 2024, there have been more than 2100 Profiling biogeochemical (BGC) Argo floats that

63   provide ocean oxygen observations with unprecedented temporal and spatial resolutions in this century (Johnson et al.

64   2017; Roemmich et al. 2019).

65   Different techniques have been applied in the past to collect ocean oxygen data, and the total number of oxygen

66   profile data from all instrument types within the World Ocean Database (Boyer et al., 2018) reached a total of more than

67   1.2 million by 2023. However, there are a lot of data quality issues in the historical oxygen database due to many

68   reasons, including instrumental errors, data collection failure, data processing errors, improper sample storage, unit

69   conversion and others. Furthermore, as different instruments have different data quality, merging several

70   instrumentation types into an integrated database requires proof of data consistency.

71   These quality issues impede the various applications of oxygen data, for instance, investigating how much oxygen

72   the ocean has lost in the past decades (Levin et al., 2018; Gregoire et al., 2021). Previous assessments indicate the

73   decline of open ocean full-depth O_2 content of 0.3%~2% since the 1960s, with an upper 1000 m O_2 content decrease of

74   0.5–3.3% *(0.2–1.2 μmol kg^{-1} dec^{-1})* during 1970–2010 (Gulev et al. 2023). The maximum estimate is at least 6 times

75   larger than the minimum one, suggesting substantial uncertainty in quantifying the open ocean oxygen changes, which

76   is a grand challenge for the accurate assessment of deoxygenation (Helm et al. 2011; Long et al. 2016; Ito et al. 2017;

77   Schmidtko et al. 2017; Breitburg et al. 2018; Sharp et al. 2023). Furthermore, there is a mismatch between observed and

78   modelled trends in dissolved upper-ocean oxygen over the last 50 years (Stramma et al. 2012). Uncertainties and

differences between estimates are at least partly attributed to the oxygen data quality issues and inconsistency introduced by different instrument types (e.g. different precision, instrument-specific errors/biases) (Gregoire et al., 2021). For example, some BGC-Argo data conduct in-air oxygen measurements which can be used to correct potential systematic errors, while in other cases a climatology isd used (i.e. World Ocean Atlas) as a reference (Bittig and Körtzinger, 2015; Gregoire et al., 2021). Therefore, a consistent and thorough assessment of oxygen data quality, including a uniform data quality control for all instruments and instrumental bias assessments/corrections, is critical to providing a homogeneous ocean oxygen database for various follow-on applications, including quantification of the trend of ocean deoxygenation.

The paper aims to provide a quality-controlled (QC-ed), consistent global oxygen dataset for the entire period 1920-2023. To achieve this goal, a novel automated QC procedure for ocean oxygen profiles was developed. We implement this QC procedure in the global archive and analyze and describe the quality of oxygen data obtained by different instrumentation types. The performance of the quality control procedure is assessed using subsets of high-quality hydrographic data and the QC-ed BGC Argo float profiles. Finally, using bottle sample data obtained through the Winkler method as a reference, we assess oxygen biases for ship-based CTD and BGH Argo oxygen profiles.

The rest of the paper is organized as follows. The data and methods employed in the study are presented in Section 2. The data QC procedure is introduced in Section 3, with the data quality assessment presented in Section 4. The results of the benchmarking of the automated QC procedure using manually controlled datasets are shown in Section 5. Assessment of the residual bias for Argo and CTD profiles is conducted in Section 6. Data availability is described in Section 7. The results of the study are summarized and discussed in Section 8.

2   Global archive of dissolved oxygen profiles

The original oxygen profile data at observed levels are sourced from two large depositories: 1) World Ocean Database (as of January 2023) and 2) Oxygen profiles from the Argo Global Assembly Center (GDAC) (ARGO, 2000). World Ocean Database (Boyer et al., 2018) represents the largest depositary of the dissolved oxygen profile data. For the current study we used ship-based WOD oxygen data coming from two main instrumentation types: 1) Ocean Station Data (OSD) and 2) high-resolution CTD profiles. OSD instrumentation group is represented by bottle casts with oxygen determined by the Winkler method. CTD profiles are obtained mainly through the electrochemical sensors. For the Argo float data from GDACs both raw (unadjusted) and adjusted and QC-ed data are available with the latter used for the study.

The OSD profiles are most abundant between the 1960s to 2000s, CTD profiles between the 1990s to 2010s, and Argo profiles dominate after 2010 (Fig. 1). The geographical distribution of oxygen profiles is inhomogeneous (Fig. 2), with OSD profiles exhibiting almost global coverage compared to CTD and Argo, with dense sampling typical for the near-coastal areas and a sparser sampling in the central parts of the oceans (Fig. 2a). The CTD profiles are most abundant in the North Atlantic Ocean and are represented by a sparse net of transoceanic sections in the central parts of the main ocean basins, leaving large data gaps especially in the central regions of Pacific, Indian, and Southern oceans (Fig. 2b). The total number of profiles from all three groups exceeds 1.2 million for the time period 1920 to 2023, so manual QC of the global oxygen dataset is nearly impossible.
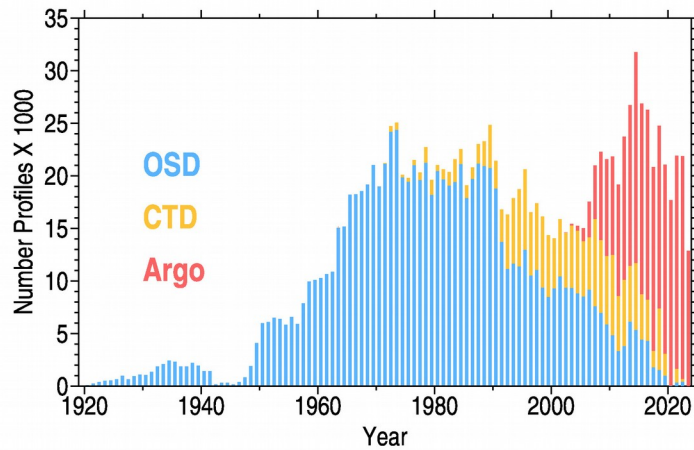
Figure 1. Yearly number of oxygen profiles from the World Ocean Database (OSD and CTD profiles) and national DACs (Argo) from 1920 to 2023.

116

117   Number of oxygen profiles disseminated by ten national Argo DACs and used for the current study is given in

118   Table 1. The most considerable contribution comes from two DACs: the Atlantic Oceanographic and Meteorological

119   Laboratory (AOML) and the French CORIOLIS Center (Coriolis). Together, these two DACs contribute 71% of all

120   oxygen profiles. The global sampling by Argo floats is characterized by big gaps in the tropical belt of the World Ocean

121   (Fig. 2c) and in the marginal seas with shallow bottom depths.

122   The DACs report oxygen data along with quality flags set after the QC procedure performed in each DAC. The

123   spatial distribution of the profiles from each DAC is shown in Fig. 3. Only the AOML dataset is characterized by a

124   more or less global coverage. The profiles from the second large Coriolis dataset are concentrated mostly in the Atlantic

125   and Southern oceans. Other DACs are characterized by a regional scope: JMA data come from the Pacific Ocean east of

126   Japan, CSIRO profiles cover the Southern Ocean, CSIO mainly provides profiles in the subtropical and tropical western

127   Pacific Ocean, and BODC profiles are located in the Atlantic Ocean. Profiles from KORDI and KMA, the smallest two

128   datasets, are located in the southern part of the Sea of Japan.

129

130   **3 Data quality control**

131   Quality evaluation of hydrographic data typically consists of two parts: data QC for random errors and evaluation

132   of systematic errors or biases. These two issues are often treated separately but represent the entire QC procedure. A

133   unified QC procedure has yet to be suggested for the global archive of oxygen profile data, and oxygen-related studies

134   often rely on WOD (Garcia et al., 2018), Argo (Thierry et al., 2021) and Bushnell et al., (2015) QC procedures. The

135   efforts undertaken under the International Quality-Controlled Ocean Database (IQuOD) initiative (Cowley, 2021)

136   resulted in a comprehensive study where different quality control procedures for temperature profiles were compared

137   and evaluated (Good et al., 2022). As shown in the previous section, the characteristic feature of the global oxygen data

138   archive is its heterogeneity. In the early years, a relatively small amount of data permitted expert quality control, but for

139   the actual global archive, automated quality control procedures (AutoQC) are required.
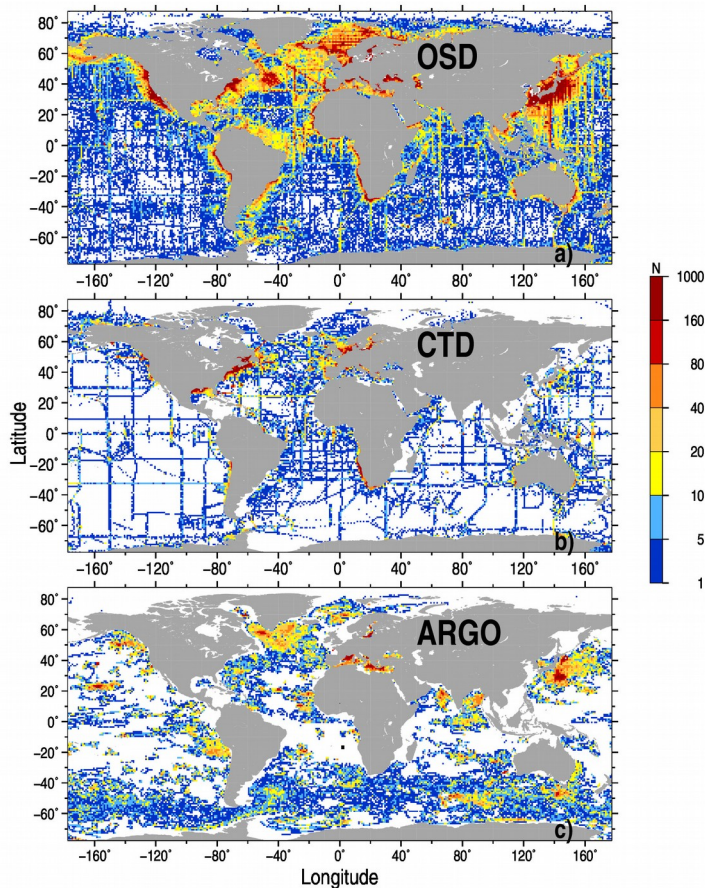
Figure 2. Number of profiles (N) in 1°×1° latitude/longitude squares for OSD (a), CTD (b), and Argo (c) data

140

141   The AutoQC procedure aims to identify and flag outliers, which represent observations significantly deviating

142 from the majority of other data in the population. Monhor and Takemoto (2005) noted that there is no rigid

143 mathematical definition of an outlier. The outliers do not necessarily represent erroneous measurements and can occur

144 due to the natural variability of the measured variable. A QC procedure defines outliers using a set of thresholds, which

145 are based on physical laws (for instance, the maximum solubility of gases in the water) or have to be defined based on

146 the statistical properties of the data population.

147   In this paper, we introduce a novel QC procedure capable of conducting quality assessment of data from different

148 instrumentation types. The procedure is applied to the observed level data and does not require additional quality checks

149 for profiles interpolated at a predefined set of levels. This second level of QC is an attribute of the WOD QC system

150 (Garcia et al., 2018). To increase the reliability in detecting erroneous data, a set of quality-checks is applied to each

151 profile. The larger the number of failed distinct quality checks, the higher the probability that the flagged observation

152 represents a data outlier. Based on the available QC schemes for oceanographic data (most of them were developed for

153 temperature and/or salinity profiles), quality checks can be subdivided into the following groups:

154 Group-1. Check of location, date and bottom depth of the profile.

155 Group-2. Check of profile attributes (maximum sampled depth, number of levels, variables measured) correspond to

156 the attributes of the instrumentation type.

157 Group-3. Range check, e.g., comparison of observations at each level against minimum/maximum value thresholds,

158 which are set for the entire ocean, oceanic basin (global ranges) or for the particular location and depth).

159 Group-4. Check of the profile shape, which is characterized by the vertical gradient of the measured variable at

160 observed levels, by the number of local extrema, and by the presence of spikes.

161

162 It should be noted that QC procedures often assume Gaussian distribution law, and outliers are defined in terms of

163 multiple times the standard deviation from the mean value (Z-score method). For instance, the WOD standard deviation

164 check is based on this assumption (Garcia et al., 2018; Boyer et al., 2018). However, distributions of oceanographic

165 parameters are typically skewed, and the assumption of Gaussian distribution leads to false data rejection. Tukey (1977)

166 introduced a so-called box-plot method, which makes no assumption about the distribution law and is often used for

167 outlier detection. Hubert and Vandervieren (2008) developed the adjusted Tukey's boxplot method for skewed

168 distribution with fences depending on skewness. Following this approach, Gouretski (2018) and Tan et al. (2023)

169 applied QC checks, taking into account the skewness of temperature distribution. In the current study we use the Hubert

170 and Vandervieren (2008) adjusted boxplot method as modified by Adil and Irshad (2015).

171

172 **Table 1**. Argo oxygen profiles from different national DACs.

N	National Data Assembly Center	Code Name	Number of Argo profiles	Number of Argo profiles collocated with Winkler profiles	Percent of Argo profiles having collocations with Winkler profiles
1	Atlantic Oceanographic and Meteorological Laboratory, US	AOML	89059	32396	41.08
2	CORIOLIS data Center, France	Coriolis	63220	33233	65.09
3	Commonwealth Scientific and Industrial Research Organization, Australia	CSIRO	19183	3302	23.75
4	Japan Meteorological Agency, Japan	JMA	15981	11233	82.90
5	Indian National Centre for Ocean Information Services, India	INCOIS	9901	2069	33.09
6	Second Institute of Oceanography, Ministry of Natural Resources, China	CSIO	6455	3921	68.98
7	Marine Environmental Data Service, Canada	MEDS	4605	14.04	50.50
8	British Oceanographic Data Center, UK	BODC	3533	1905	61.57
9	Korea Ocean Research and Development Institute, Korea	KORDI	2239	0	0
10	Korea Meteorological Administration, Korea	KMA	93	0	0

173

174
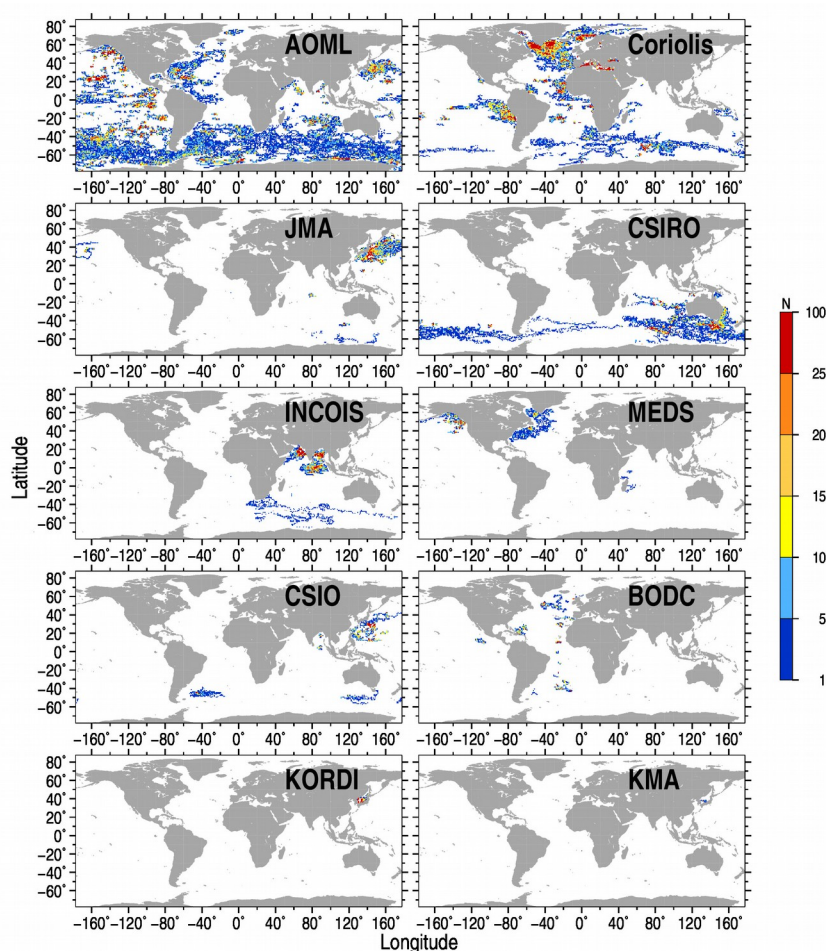
Figure 3. The number (N) of Argo oxygen profiles in 1°×1° spatial boxes for the datasets from different DACs. The name of each DAC is shown on Asia.

175   Developing the QC procedure, which consists of a suite of distinct checks, we assume that oxygen data obtained

176 by the reference Winkler method are superior in their quality compared to the sensor data. As noted by Golterman

177 (1983), the principle of the Winkler method has been unchanged since its introduction, with the method still providing

178 the most precise determination of dissolved oxygen. There is a total of ten distinct quality checks, which are introduced

179 in sections 3.1 to 3.9. The outlier statistics are shown in the respective supplements (Fig. S1-Fig.S10) both for the year/

180 depth bins and within 2°×4°geographical boxes along with randomly selected oxygen profiles affected by the respective

181 check.

182 **3.1   Geographical Location Check**

183   A comparison of the deepest sampled level with the local ocean bottom depth may be used for the identification of

184 erroneous geographical locations. We use GEBCO 0.5-minute resolution digital bathymetry map to define thresholds

185 for this check. For each profile, the range between minimum and maximum GEBCO bottom depth within the 111km

186 radius is calculated. If the difference between the deepest profile measurement depth and the local GEBCO depth

187 exceeds the above depth range, the geographical coordinates of the profile are considered to be in error and data at all

188 levels are flagged. According to Table 2 about 0.5% OSD and CTD profiles fail this check, compared to only 0.08% for

189   Argo profiles. For each data types the spatial distribution of profiles failing this test exhibits a rather random pattern

190   (Fig.S1). The highest percentage of OSD outlier profiles are found for the time period before 1946, probably due to less

191   accurate navigation methods during the war (Fig.S1b). CTD profiles exhibit higher outlier scores above 400 m between

192   200-2014 linked to several cruises. Only 0.077% of DAC QC-ed Argo profiles fail this check (Fig.S1g-i).

3.2   Global oxygen range check

194   The test is applied to identify observations that are grossly in error (the so-called 'blunders'). These data

195   correspond to the cases of the total instrumentation fault or crude errors introduced during the data recording or

196   formatting. The overall minimum/maximum oxygen ranges are defined based on the entire archive of the OSD profiles.

197   These overall ranges are set for depth levels and temperature surfaces because the maximum oxygen solubility depends

198   on temperature. For the construction of overall limits, we use the normalized frequency histograms (Fig. 4). The

199   depth/oxygen histograms are constructed similarly with normalization at each depth level (Fig. 4b). The normalization

200   is done to account for varying numbers of oxygen observations with depth and temperature. The relative frequencies

201   serve as the guidance to produce the overall oxygen minimum and maximum limits, which approximately correspond to

202   the relative frequency of 0.05 (indicated by the green lines). Spatial distribution of the OSD and CTD profiles with

203   levels failing this check broadly corresponds to the sampling density (FigS2a, d and Fig. S3a, d), whereas flagged Argo

204   profiles can be rather linked to distinct floats (Fig. S2g, Fig. S3d). The CTD data are characterized by the largest

205   fraction of profiles affected by this check (Fig. S2e, Fig. S3e).

206
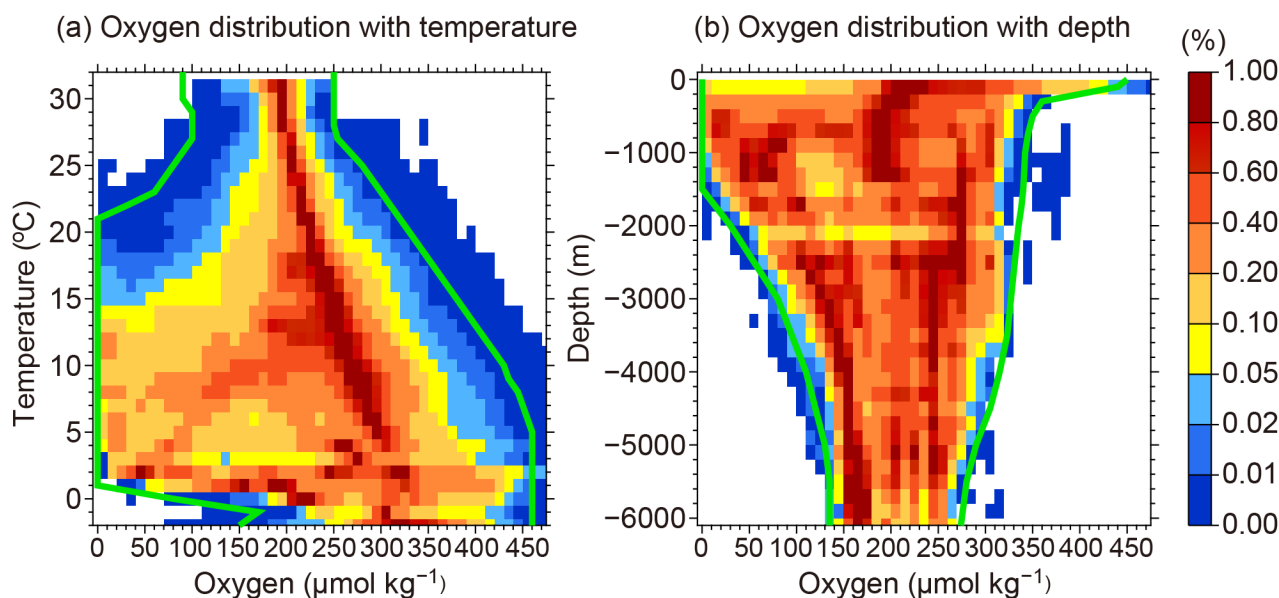
Figure 4. Normalized oxygen histograms used to define overall oxygen ranges versus temperature (a) and versus depth (b). Minimum and maximum overall oxygen limits are shown by solid green lines. For each temperature/oxygen bin in (a), the number of oxygen observations is divided by the number of observations in the most populated bin for the same temperature. The depth/oxygen histograms (b)are constructed similarly with normalization at each depth level.

208

3.3   Maximum oxygen solubility check

210   According to Henry's law, the quantity of an ideal gas that dissolves in a definite volume of liquid is directly

211   proportional to the partial pressure of the gas. It is also known that gas solubility in the water typically decreases with

212   increasing temperature. The histograms between observed oxygen concentration (C_{obs}) and maximum oxygen solubility

213 (C_{max}) calculated using reported temperature and salinity at different ocean layers depict a close relationship between the

214 mode of observed oxygen distribution and the maximum solubility (Fig. 5a-d). The histograms also show that the

215 distribution mode for the upper-most layer 0-100 m (Fig. 5a) follows the line $C_{obs} = C_{max}$ progressively deviating to

216 lower C_{max} values when $C_{obs} > 300$ µmol kg^{-1}, suggesting an oxygen super-saturation. That is because, in the photic layer

217 of the ocean, oxygen is produced by phytoplankton through photosynthesis, and oxygen super-saturation can evolve.

218 Oxygen production due to photosynthesis leads to the formation of small bubbles (10-70 micron) with increasing

219 oxygen super-saturation accompanied by a higher number of bubbles and their shift towards large sizes (Marks, 2008).

220 In the deeper layers (Fig. 5b-d), the number of cases with super-saturation decreases because of the reduced

221 photosynthesis, so the temperature and pressure effects dominate. According to the histograms (Fig. 5a-d),

222 supersaturation is frequently observed in the upper layers. The percentage of supersaturated values decreases from

223 about 45 % in the near-surface layer to less than 1.0 % below the 200 m level (Fig. 5e, red).

224
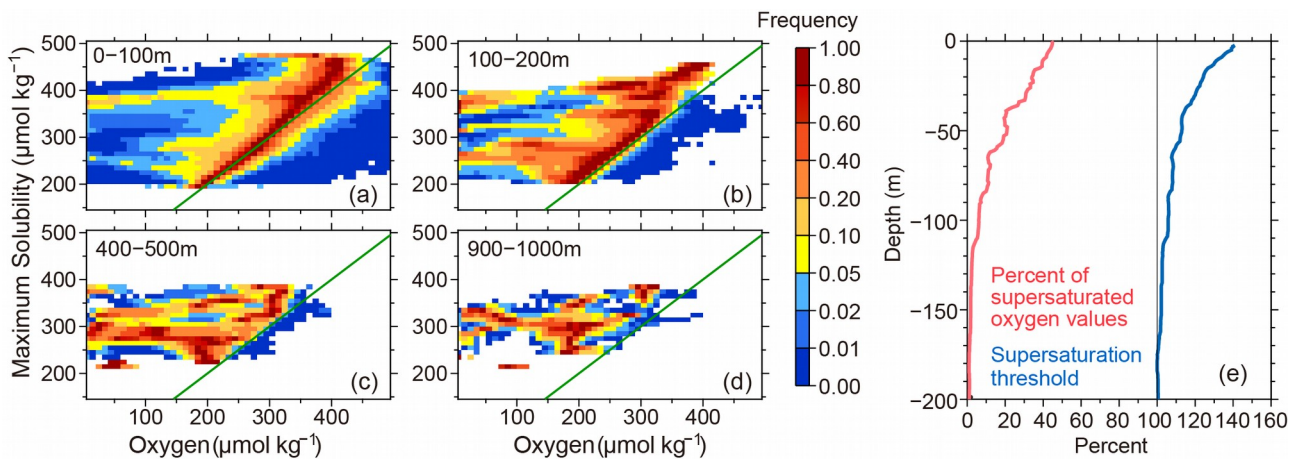
Figure 5. Super-saturation check: (a-d) normalized frequency histograms for maximum solubility versus reported dissolved oxygen value for different layers. The bin size is 10 µmol kg^{-1}. For each maximum solubility level, the frequencies for each bin are normalized by the number of the values in the most populated bin in order to account for variations in the number of profiles. (e) percentage of supersaturated oxygen values over all observed oxygen values (red) and the threshold for the super-saturation check, represented by the percentage relative to the maximum solubility (blue).

225

226   In order to set the threshold percentage for super-saturation we calculated histograms of super-saturation values for

227 each 1-meter depth level of the upper 500 m layer. The threshold percentage of super-saturation (Fig. 5e, blue line)

228 corresponds to the 99th quantile. The threshold value approaches 100% near the depth of 200m, therefore, below 200 m

229 all supersaturated oxygen values are flagged. Locations of profiles with at least one observed level failing this check are

230 shown in Fig. S4a, d, g. The distribution of profiles broadly corresponds to the spatial sampling density. The OSD

231 outliers are more numerous in the early years before 1955 probably pointing to less accurate measurements during that

232 time period. The check reveals a much higher percentage of CTD outliers throughout the water column for several years

233 before 2000 (Fig. S4b) compared to other instrumentation types. Argo floats are characterized by the low outlier

234 percentage for this quality check with a higher percentage found for deep Argo floats between 2017-2018 below 2000m

235 (Fig. S4h).

236

3.4 Stuck value check

Malfunctioning of sensors often results in stuck values when the same oxygen concentration is reported for all or most of the observed levels. To identify such profiles, we calculated oxygen standard deviations for each oxygen profile to build histograms (**Fig. 6)** for each instrumentation type. Only profiles with at least seven oxygen levels are considered. Unlike the OSD and Argo data, for which the frequency of profiles drops for low standard deviation values, the CTD profiles are characterized by a distinct peak for the lowest standard deviation values (Fig. 6c). Accordingly, based on the histograms (Fig. 6b, c), we set the thresholds of 3 µmol kg^{-1} and 1 µmol kg^{-1} and for CTD and PFL profiles, respectively. No lowest value thresholds are applied for OSD profiles, as stuck values are characteristics of the electronic sensors only. Geographical distribution of profiles failing this check is given by the Fig. 5a, d. The check is applied only to the CTD and Argo sensor data. Check reveals high percentage of outliers for CTD profiles especially after 2000 (Fig. 5b). Argo profiles which fail the check are not numerous and located mostly in the Northern Hemisphere (Fig. 5d).
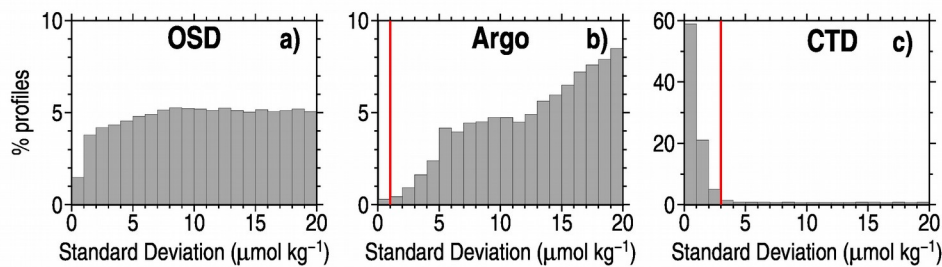
Figure 6. Oxygen profile standard deviation for OSD (a), Argo (b), and CTD (c) instrumentation types. Only profiles with at least five levels of oxygen data are considered. Red vertical lines show the respective threshold values for Argo and CTD profiles.

3.5 Multiple extrema check

Multiple extrema check aims to identify profiles whose shape significantly deviates from the majority of profiles. The definition of the extrema and the checks are illustrated in Fig. 7a. For each profile with at least 7 observed levels (black dots), the number of local extrema and their magnitudes (denoted as M_n in Fig.7a, defined as oxygen difference between two adjacent oxygen measurements) are calculated. Then, the normalized frequency histograms of oxygen profiles for different combinations of the number of oxygen extrema and of the extremum magnitude are calculated for three instrumentation types separately (Fig. 7b-d). The larger the extremum magnitude, the less frequent the corresponding profiles. Physically, an oxygen profile at a location is not likely to exhibit too large and too frequent oscillations of oxygen concentrations. Thus, the profiles with many/big extrema are likely erroneous. The histogram for Argo profiles differs from those for OSD and CTD because it is based on profiles already validated by the respective DACs. The Multiple extrema check thresholds (black lines in Fig. 7b-d) are defined using the histograms as the guidance. The lines crudely correspond to the normalized frequency of 0.01 for OSD and CTD and 0.05 for PFL profiles. The geographical distribution of profiles failing the check is given in Fig. S6a, d, g. Argo profiles failing the check can be linked to distinct floats (Fig. S6g). The OSD profiles exhibit a higher outlier percentage for the years 1990-2002. The highest rejection rate for the CTD profiles is typical for the years before 2000 (Fig. S6b, e).
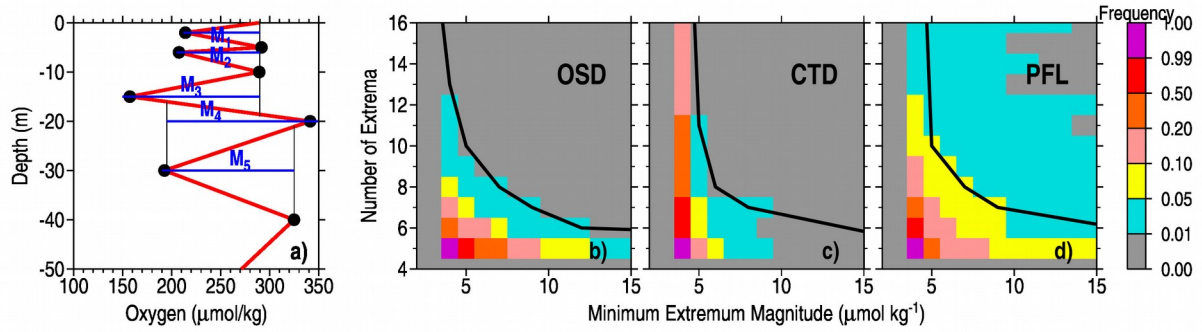
Figure 7. (a) Schematics for the multiple extrema check. Black dots represent the observed values, and the local extrema is defined by M, whereas extremum magnitudes are shown with blue lines. (b-d) Normalized frequency histograms for multiple extrema checks for OSD (b), CTD (c), and PFL (d). The area to the right of the black line corresponds to oxygen profiles failing the multiple extrema check.

266

3.6 Spike check

268   Spikes are the values at levels that strongly deviate from the values at the nearest levels above and below. For each
269   observed level k, the test value $s = s_1 - s_2$ is calculated, where $s_1 = |p_k - 0.5 (p_{k-1} - p_{k+1})|$, $s_2 = |0.5 (p_{k+1} - p_{k-1})|$ and p denotes
270   the oxygen value. The observation is identified as outliers when the test value s exceeds a threshold value. Due to the
271   larger natural oxygen variability in the upper layers, we set depth-dependent spike thresholds, which are defined for
272   nine depth layers using accumulated histograms for the test value s (Fig. 8a, b for 0-100m, 400-600m as examples). The
273   threshold profile is defined by the 95% frequency at each layer (Fig. 8c). The value is chosen empirically but can be
274   tuned when additional QC-ed benchmark datasets become available. Examples of profiles which failed this check are
275   shown in Fig 7S. Data from all instrument types are characterized by a rather homogeneous temporal and spatial
276   distribution of outliers.

277
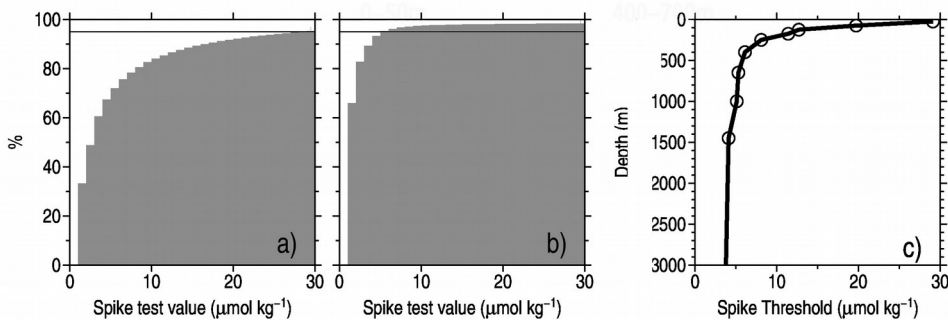
Figure 8. Spike test value histograms (see text for details) for the layer 0-100m (a) and 400-600m (b); spike test value threshold versus depth (c).

3.7   Local Climatological Oxygen Range Check

279   Local climatological oxygen range check is one of the most effective QC modules to identify outliers compared to
280   other checks because the minimum/maximum thresholds are constrained by the local water mass characteristics. For
281   each 1°×1° latitude/longitude grid point, we calculate min/max thresholds, accounting for the skewness of the data. For
282   calculating climatological ranges, we take the ergodic hypothesis in which the average over time is considered to be
283   equal to the average over the data ensemble within a certain spatial influence radius. Taking into account the skewness

284 of statistical distribution when defining climatological ranges for oceanographic parameters was first suggested by

285 Gouretski (2018), who applied Tukey's box plot method modified for the case of skewed distributions (Hubert and

286 Vandervieren, 2008; Adil and Irshad, 2015). In this method lower (Lf) and upper (Lu) fences are calculated according

287 to formula (1):

288

289 [Lf Uf] = [Q1 – 1.5*IQR*exp(-SK*|MC|)   Q3 + 1.5*IQR*exp(SK*|MC|)],   (1)

290

291 where Q1, Q3 are quartiles, Q2 is sample median, SK is skewness. MC denotes medcouple, which is defined as MC =

292 median $h(x_i,x_j)$, where $x_i << Q2 << x_j$; and the kernel function $h(x_i,x_j) = [(x_j-Q2)-(Q2-x_i)]/(x_j-x_i)$. (Hubert and

293 Vandervieren, 2008).

294   The local oxygen ranges are constructed using both the OSD and Argo oxygen profiles. The OSD data used to

295 derive the local threshold have undergone the preliminary QC (checks for overall oxygen range, spikes, stucked value,

296 multiple extrema), aiming to remove crude outliers to reduce their impact on the local thresholds. This approach is

297 similar to the two-stage thresholding suggested by Yang et al. (2019). The Argo oxygen profiles underwent quality

298 control at the respective DAC centres.

299   The local minimum and maximum thresholds were calculated at 1x1-degree grids at a set of 65 depth levels

300 corresponding to the levels implemented for the World Ocean Experiment/Argo Global Hydrographic Climatology

301 (Gouretski, 2018) using formula (1). Examples of the threshold spatial distribution are presented for two depth levels:

302 98 meters (level typically located below the seasonal thermocline, Fig. 9a-c) and 1050 m (level typically located below

303 the main thermocline, Fig.9 d-f). The most striking features are the areas with low minimum oxygen values (oxygen

304 minimum zones, Fig. 9 a, b) in the East Pacific, Arabian Sea, Bay of Bengal, Black Sea, and Baltic Sea. The oxygen

305 range map for level 98 m (Fig. 9c) shows that the areas with the widest local ranges coincide with minimum oxygen

306 zones. The local range map for the 98 m level also depicts wider ranges in several highly dynamic regions of the Gulf

307 Stream, Malvinas current, and the area north of the Antarctic coast (Fig. 9c). During the QC, gridded minimum and

308 maximum local oxygen values are interpolated to the observed levels at profile locations. The geographical distribution

309 of profiles failing the check is given in Fig. S8a, d, g , indicating a rather uniform temporal and spatial distribution. A

310 decrease with time of the outlier percentage for OSD data is clearly seen. For CTD data the outlier percentage is high

311 for all levels and years except for the years after 2020. Argo profiles failing the check in many cases can be linked to the

312 data from particular floats (Fig. S8g).

313 **3.8   Local climatological oxygen gradient range check**

314   The oxygen vertical gradient check aims to identify pairs of levels for which the vertical oxygen gradient exceeds a

315 certain threshold. Threshold values for the vertical gradient (Fig. 9 i-n) are calculated using formula (1), similar to the

316 local oxygen ranges. Due to the nonlinearity of oxygen profiles, vertical gradient values depend on the profile's vertical

317 resolution, e.g., from the gap between two neighbors' observed levels. Respectively, oxygen thresholds have been

318 calculated for several depth gaps between 10m and 100m, as Tan et al. (2023) did for the QC of temperature profiles.

319   For level 98 m, the spatial distribution of the oxygen gradient range (Fig. 9k) is similar to the spatial pattern of the

320 oxygen range (Fig. 9c), with the largest ranges located in the oxygen minimum zones, reflecting the highest oxygen

321 variability in these areas. The region below the main thermocline (Fig. 9 l-n) is characterized by a much smaller range

322 compared to the 98m level. The geographical distribution of profiles failing the check is given in Fig. S9a, d, g,

 indicating a rather uniform temporal and spatial distribution broadly corresponding to the sampling density. For CTD

324 data the lowest outlier percentage is observed after 2000 (Fig. S9e).
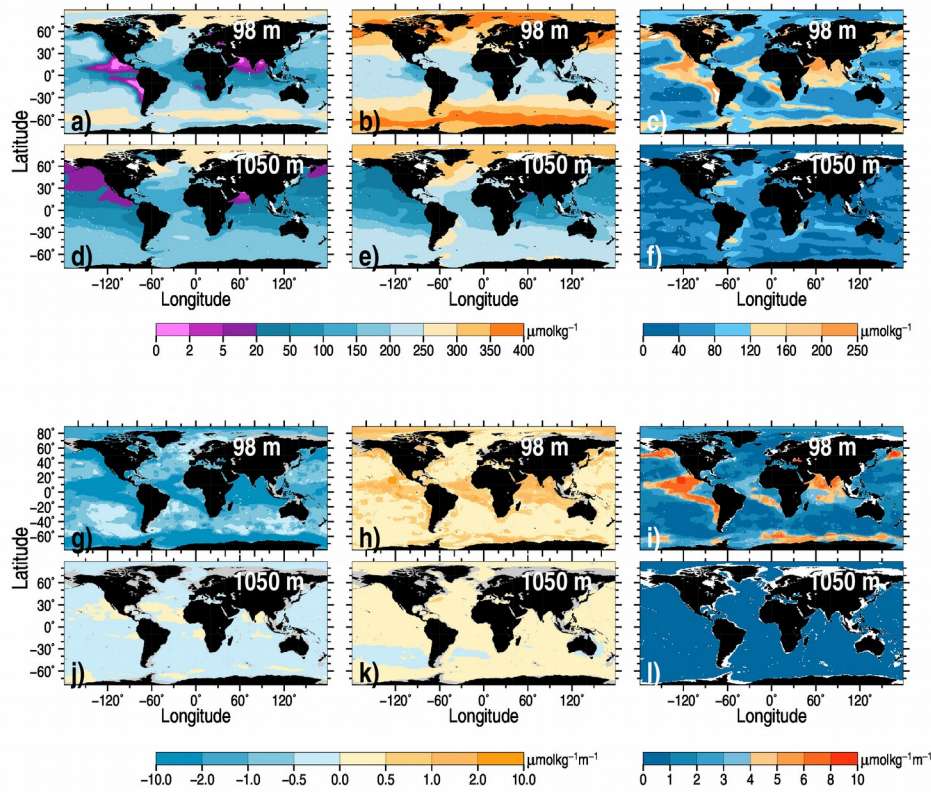
Fig.9. Upper six panels: maps of the lower (a), the upper (b) climatological oxygen threshold and of the oxygen range (c) for the 98m depth level; d-f) same but for the 1050 m depth level. Lower six panels: maps of the lower (g), the upper (h) climatological oxygen vertical gradient threshold and of the oxygen vertical gradient range (i) for 98 m depth level; j-l) same but for the 1050 m depth level.

325 **3.9   Excessive flagged level percentage check**

326   After applying all previous quality checks, the percentage of flagged levels for each oxygen profile is calculated to

327 produce histograms in **Fig. 10**. A threshold is set based on these histograms to decide on the quality of the entire profile:

328 we set 20%, 15%, and 30% thresholds for OSD, Argo, and CTD profiles, respectively. If the threshold is exceeded, the

329 entire profile is flagged, and it is suggested that it not be used in future analyses. Both the OSD and Argo datasets are

330 characterized by a low number of profiles with a high percentage of flagged data. In contrast, for the CTD group, the

331 histogram (Fig. 10c) exhibits a thick and long tail with a significant fraction of profiles having a high percentage of

332 flagged levels.

333   The geographical distribution of profiles failing the check is given in Fig. S10a, d, g, indicating a rather uniform

334 temporal and spatial pattern. A decrease of the outlier percentage with time for OSD data is seen after about 2005 (Fig.

335 S10b). For CTD data the outlier percentage is high for all years except 2021. Argo profiles failing the check in many

336 cases can be linked to distinct floats (Fig. S10g).
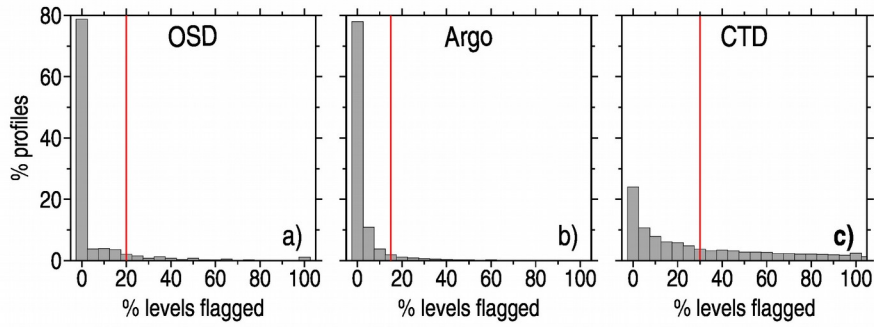
Fig.10. Percentage of oxygen profiles versus percentage of rejected levels per profile for OSD (a), CTD (b), and Argo (c) instrument types.

4 Evaluation of the QC procedure

Table 2 and **Fig. 11** summarize the rejection rates for all ten quality checks for the three instrumentation types separately. The Argo oxygen profiles have the lowest overall rejection rate of 4.8%, with Winkler data quality ranking second best (12.0% outliers). The difference might originate from 1) Winkler profiles cover a century-long period of observations, with a poor data quality in the earlier decades; 2) the analyzed Argo oxygen data are represented by adjusted profiles, which have been already quality-controlled.

Figure 11. (a-c) Percen of measurements flagged by distinct quality checks for three instrumentation types; (d-f) percent of
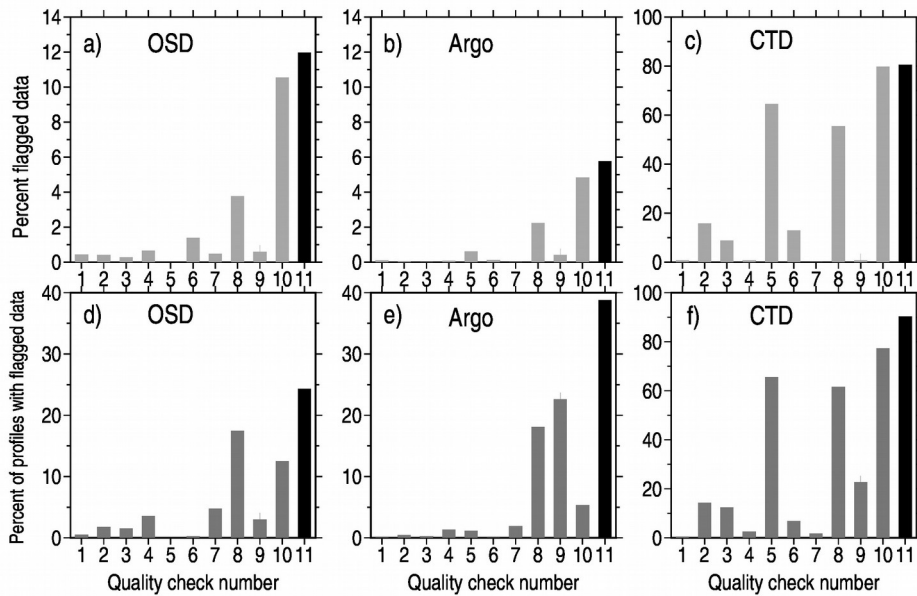
profiles with at least one measurement flagged. For the description of checks see Table 2. The black bar at the number 11 corresponds to the total percent of flagged data (a-c) and to the percent of profiles flagged by at least one quality check (d-f).

The CTD oxygen profiles have the highest percentage of outliers (overall rejection rate of 90.0%). The significant part of CTD oxygen outliers is attributed to the profile standard deviation check, which searches for profiles with identical or very similar oxygen values at all observed (reported) levels (Fig, 11a, check-5). Most of these profiles also fail the local climatological range check. We note that these profiles have also been identified as outliers during the

349 compilation of the WOA18 (Garcia et al., 2018) and WOA23 (Reference) atlases of dissolved oxygen and have not

350 impacted climatological oxygen distributions presented in these atlases.

351   As introduced above, the local climatological range check (Check-9 in Table 2) represents the most important

352 quality check and results in the highest percentage of flagged observations and profiles. For OSD, about 24% of profiles

353 have at least one measurement flagged by this check. For Argo and CTD profiles, these values are 36.8% and 90.0%,

354 respectively.

355   **Fig. 12** shows the percentage of flagged measurement versus time and depth and within one-degree

356 latitude/longitude boxes for three main instrumentation types. The OSD group exhibits a graduate decrease of outlier

357 percentages with time at all depths (Fig. 12a), indicating the gradual improvement of data quality with time, especially

358 after the early 1990s, which coincides with the beginning of the extensive observational activities during the World

359 Ocean Circulation Experiment (WOCE). The global spatial pattern of outliers (**Fig. 12b**) is characterized by outlier

360 percentages lower than 5% in most 1° grid cells, with only a few areas exhibiting higher percentages, which can be

361 linked to some particular cruises or observational programs.

362   Oxygen data from Argo floats (**Fig. 12c, d**) are characterized by a low percentage of outliers reflecting the impact

363 of the *QC* and data adjustments already conducted at DAC centres. We also find no clear time trend in outlier scores.

364 There is an indication of higher outlier percentages in the layer below 1500 m before 2020 (**Fig. 12c**). Strong spatial

365 contrasts in the percentage of Argo outliers (**Fig. 13d**) in most cases can be linked to particular Argo floats.

366   Unlike the OSD Winkler data, CTD oxygen profiles do not suggest a time trend in data quality (**Fig. 12e**).

367 Compared to both OSD and Argo, ship-based CTD oxygen profiles are characterized by a much higher outlier

368 percentage. This is explained through a significant fraction of CTD profiles failing the standard deviation check, the

369 multiple extrema check, and overall global range checks. The CTD outlier profiles are evenly distributed over the

370 oceans (**Fig. 12f**). **Fig.12g, h** shows outlier distributions for the profiles which passed both the standard deviation and

371 the multiple extrema checks. In this case, most cruise lines (**Fig. 12h**) are characterized by a low outlier percentage,

372 with data quality issues related to a smaller subset of cruises. Finally, we find that the CTD data since 2018 (**Fig. 12g**)

373 exhibit very low outlier scores comparable to those of OSD and Argo float profiles.
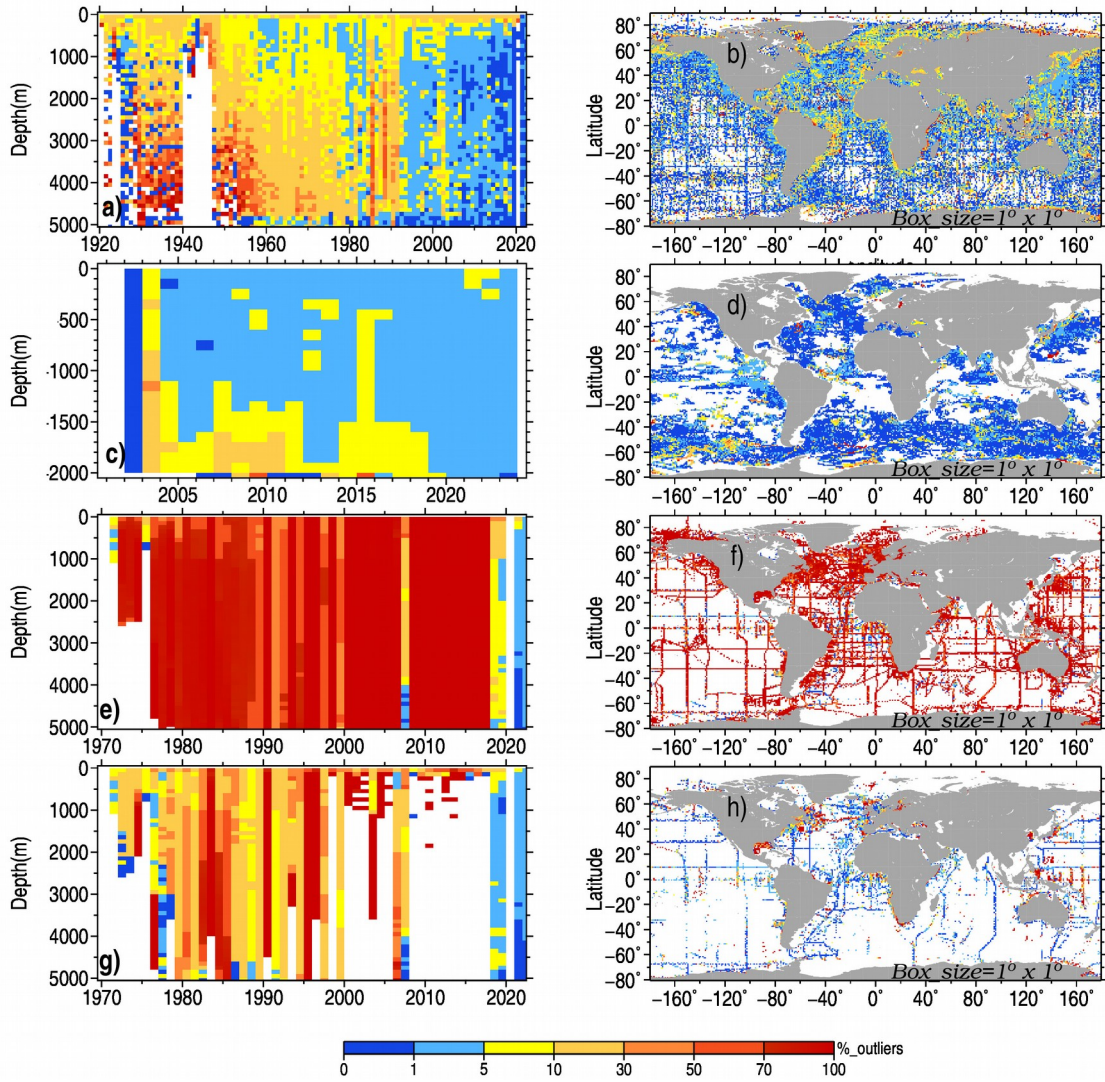
Fig.12. Percentage of flagged observations in year/depth bins (a) and in $1°$ latitude/longitude boxes (b) for OSD oxygen profiles; (c) and (d) same but for Argo oxygen profiles; (e) and (f) same but for CTD oxygen profiles; (g) and (h) same but for CTD oxygen profiles which passed multiple extrema and stuck value quality checks.

Table 2 Outlier score statistics for different instrumentation types

No.	Quality Check	OSD		CTD		ARGO	
		% flagged observations	% flagged profiles	% flagged observations.	% flagged profiles	% flagged observations	% flagged profiles
1	Location check	0.422	0.478	0.710	0.521	0.086	0.077
2	Global Oxygen Range at depth levels	0.411	1.751	15.797	14.230	0.041	0.421
3	Global Oxygen Range on T surfaces	0.270	1.492	8.824	12.379	0.009	0.227
4	Maximum oxygen solubility check	0.654	3.548	0.638	2.684	0.081	1.325
5	Stuck value check	0.000	00.000	64.547	65.504	0.043	0.073
6	Multiple extrema check	1.376	0.233	12.846	6.802	0.126	0.057
7	Spike check	0.472	4.732	0.039	1.668	0.012	1.904
8	Local climatological oxygen range check	3.766	17.453	55.398	61.513	2.232	18.118
9	Local climatological oxygen vertical gradient range check	0.584	2.962	0.103	6.207	0.181	13.743
10	Excessive flagged level percentage check	10.538	12.489	79.681	76.853	4.434	4.661
	ALL QC CHECKS	11.968	24.564	80.207	84.392	5.191	29.495

5 Benchmarking of the QC procedure using manually controlled datasets

Evaluation of the quality-control system is a crucial part of the dataset generation. Good et al. (2022) conducted a comprehensive benchmarking exercise to evaluate the performance of AQC checks for temperature profiles implemented by different research groups, aiming to recommend an optimal set of quality checks. They used several reference datasets with known quality (e.g., bench-marking datasets whose quality was manually evaluated by experts).

Unfortunately, in a deviation from temperature profiles, no community-agreed oxygen datasets exist which could be used for benchmarking. In this study, besides the examples of the QC procedure performance provided for each quality check (Section 3 and Supplementary Material), we use for the bench-marking a comprehensive set of bottle profile data obtained during the World Ocean Circulation Experiment (WOCE) – the largest international oceanographic experiment ever conducted (Wunsch, 2005). To achieve a high degree of data quality and consistency between the cruises over the entire period of observations, the WOCE Hydrographic Program Office (WHPO) issued operation manuals (WHPO, 1991), where measurement methods and procedures are described. As shown by Gouretski and Jancke, (2000), the WHPO quality requirements have been fulfilled with the WOCE hydrographic dataset representing a unique global scale high-quality collection of the whole suite of oceanographic parameters. Specifically, the mean inter-cruise oxygen offset was found to be 2.389 µmol kg^{-1}. Upon completing the WOCE, the GO-SHIP program was established in 2007 to revise the WOCE hydrographic programme by repeating several WOCE lines (Hood et al, 2010).

Applying our QC procedure to the entire WOCE dataset confirms the high quality of this unique dataset, with only 2.8% of oxygen outliers (**Fig. 13a, b**) from the total of 354028 oxygen measurements for the entire time period 1990-1998. Similar to the entire OSD dataset, the QC diagnostics reflect the progressive improvement of the oxygen data

quality over the period of WOCE (**Fig. 13a**). The spatial distribution of outliers for the entire time period (**Fig. 13c**) indicates that the majority of WOCE oxygen profiles have a very low percentage of outliers or exhibits no outliers at all. For 79% percent of WOCE oxygen profiles, our QC procedure identified no data outliers. The higher rejection rate is found only for several WOCE lines in the tropical South Atlantic, North-Western Indian Ocean, and the Labrador Sea. We note that in the same areas, there are data from other cruises which exhibit low outlier percentages, so the flagging can not be attributed to the spatial selectivity of the QC procedure.

The WOD database permits data selection for a large number of observational programs using the respective project identification code. The outlier rejection percentage for the data from 128 projects that reported oxygen data is shown in **Fig. 14.** The mean rejection rate over all projects is 7%. Apart from WOCE, several outstanding observational programs like GEOSECS (Geochemical Ocean Sections Study) (Craig, 1974), SAVE (South Atlantic Ventilation Experiment) (Larque et al., 1997), CARINA (Carbon dioxide in the Atlantic Ocean) (Falck and Olsen, 2010), and CLIVAR (Climate and Ocean: Variability, Predictability and Change) (Sarachick, 1995) delivered a significant number of high-quality hydrographic data with quality documented in the literature. We note that the four projects with a median year after 1985 (SAVE, WOCE, CARINA, and CLIVAR) are characterized by rejection rates lower than the mean. The 8% outlier rate for one of the largest international GEOSECS experiment conducted in the 1970s only slightly exceeds the mean outlier percentage over all 128 projects.

Finally, we used the delayed mode quality-controlled Argo data to evaluate the performance of our *QC* procedure. The Argo dataset used for the current study consists of oxygen profiles reported from 1794 floats. The histogram of the percentage of flagged observations for each Argo float (**Fig. 15a**) shows that for 90% of all floats the percentage of rejected observations is less than 15%, with 84% of floats exhibiting less than 5% of rejected measurements. We conclude that the *QC* applied in the DAC centers effectively identifies data outliers for the majority of the floats, resulting in a low outlier percentage (see **Fig. 12 c, d**). The location map of profiles from Argo floats with more than 15% of data flagged over the float lifetime (Fig. 15b) shows a rather random distribution throughout the world ocean, with almost all DACs contributing with such floats. We interpreted this result as an implicit confirmation of the ability of our QC scheme to identify data with quality issues.
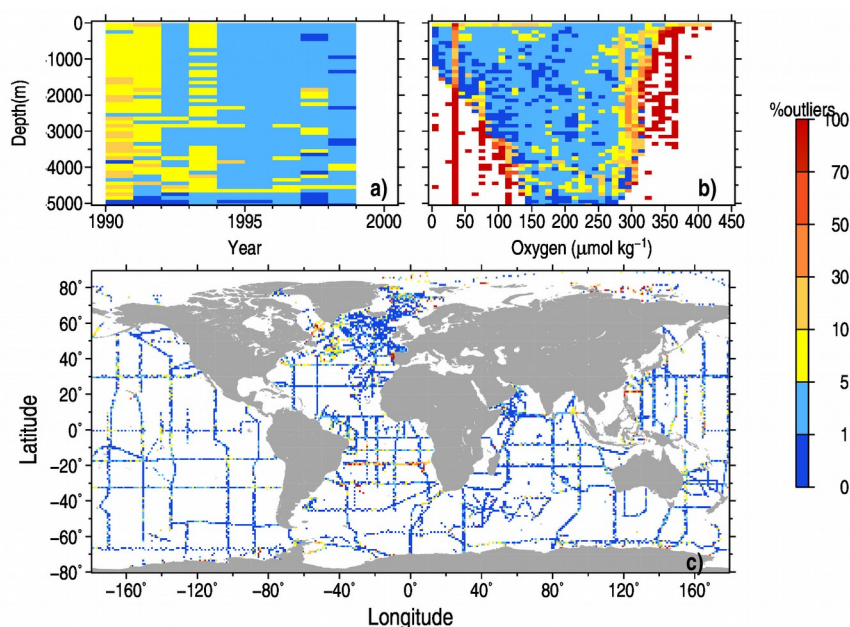
Figure 13. QC statistics for the WOCE dataset: a) percentage of outliers in year/depth bins; b) percentage of outliers in oxygen/depth bins; c) percentage of outliers in 1x1-degree squares.
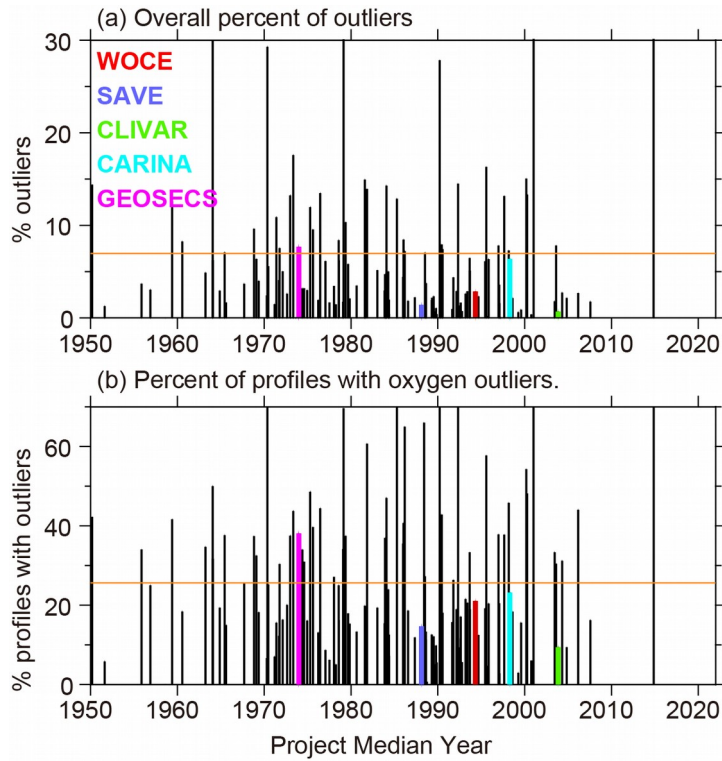
421

Figure 14. Outlier diagnostics for 128 distinct WOD projects (OSD Winkler profiles): a) overall percent of outliers; b) percent of profiles with oxygen outliers. Acronyms and percentages for selected hydrographic projects described in text are shown in color.
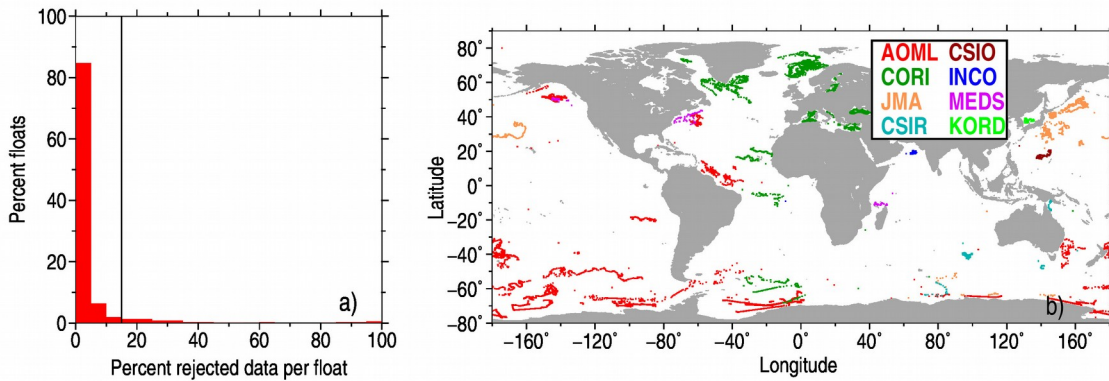
Figure 15. a) percent of Argo oxygen profiles versus percent of flagged data per profile; b) trajectories of Argo floats with more than 15% of flagged data (a total of 127 floats).

6   Bias assessment for sensor oxygen data

The QC procedure described in the previous sections is based on the underlying statistics of the data and aims to identify random outliers. The second step in data QC is estimating the possible systematic errors or biases. These systematic errors may differ depending on the instrumentation type, but the common cause for systematic errors is the absence of the possibility to calibrate the instrument. A classic example provides temperature data obtained by eXpandable bathythermographs (XBT) where systematic errors are due to the uncertainty in depth, which is calculated from the elapsed time, and the uncertainty in thermistor, which is typically not calibrated (Gouretski and Reseghetti, 2010; Cheng et al., 2014). In the case of dissolved oxygen, only Winkler oxygen determinations of discrete samples can be considered to be bias-free because the chemical analysis is based on the KIO_3 standard reference, with the replicate measurements having a precision better than 0.4 µmol kg^{-1} (Thaillandier et al., 2018). However, differences in methods and standards between hydrographic cruises suggest a lower level of data precision. Gouretski and Jancke (2000) used the high-quality WOCE one-time hydrographic dataset and conducted a comprehensive analysis of the inter-cruise oxygen differences at the cruise cross-over areas. The analysis was performed in the deep part of the water column (typically below 2000 m), where the time variations of seawater properties are small. For 305 cross-over areas, they estimated the mean difference between WOCE cruises to be 2.40 µmol kg^{-1} with a standard deviation of 2.37 µmol kg^{-1}. Considering stringent criteria for the WOCE hydrographic programme, this estimate can be considered to represent an approximate precision of the Winkler method in application to real hydrographic data. As noted by Golterman (1983), the Winkler method still represents the most precise determination of dissolved oxygen. In spite of some modifications over time, the principle of the method is unchanged. In the following, we describe residual biases for CTD and Argo profiles. The term "residual" is used because CTD oxygen profiles are typically adjusted on Winkler bottle samples, and Argo oxygen profiles used in our study undergo adjustment procedures at the respective DACs.

The use of electrochemical and optical oxygen sensors in oceanographic practice has two main aspects. First, these sensors permitted a significantly higher rate of data acquisition and a much finer vertical resolution than bottle data. Secondly, they made the observational process much easier than bottle samples, which need chemical titration in the laboratory. However, like other electronic sensors, oxygen sensors are prone to offsets and drift. Takeshita et al (2013) analyzed data from 130 Argo floats and found a mean bias of -5.0 % O_2 saturation at 100 % O_2 saturation. Bittig et al. (2018) explained this negative bias by reducing O_2 sensitivity proportional to oxygen content, with the decrease of sensitivity being on the order of several percent per year. Optode drift characteristics require regular calibration. Use of reference Winkler profiles is possible only for the ship-based CTD oxygen sensors (mostly electrochemical sensors) if CTD rosette water samples are obtained simultaneously with sensor profiles and are analyzed for oxygen during a cruise (Uchida et al., 2010). For unmanned autonomous platforms like Argo, the direct comparison with reference Winkler data is limited to samples from the hydrographic casts conducted during the float deployment. Bittig et al. (2018) recommended adjusting optode data on oxygen partial pressure primarily by the gain (Argo Quality Control Manual, 2021). If no previous delayed-mode adjustment is available, the basic real-time adjustments are performed based on the oxygen saturation maps provided by the WOA digital climatological atlas (Thierry et al., 2021). In case a delayed-mode adjustment is not available after one year, the re-assessment of the gain factor is recommended. Uncertainty in underlying optode calibration and time drift characteristics leads to errors in adjusted data.

6.1 Bias assessment method

We aim to assess the magnitude of the possible overall residual bias for CTD profiles and adjusted Argo optode profiles by comparing these profiles with collocated reference discrete samples. The data from 10 national DACs were used for this analysis, for which both unadjusted and adjusted oxygen profiles are available. Data centers and the respective number of oxygen profiles are given in Table 1. Data using Winkler method are used as reference data for the comparison with collocated Argo optode oxygen profiles.

For the current analysis, we selected a 100 km threshold distance within which two profiles are spatially collocated. To decide upon the choice of the optimal maximum time difference between Argo and reference profiles, we calculated median oxygen offsets increasing threshold value for the time separation between a pair of profiles (**Fig.16a**). Increasing the temporal collocation bubble leads to the increase of the bias magnitude in agreement with the assumption that the older reference data are richer in oxygen compared to the more recent data. Below 1000 m depth, the difference between the median offsets for the temporal collocation bubble of 5 and 50 years is about 3.5 µmol kg^{-1}, corresponding to a deoxygenation trend of about 0.7 µmol kg^{-1} per decade. This estimate can be compared with 0.75 µmol kg^{-1} per decade reported by Gregoire et al., (2021). As Fig. 16c suggests, the overall offset estimate below 1000 m stabilizes after the time difference threshold of 5 years. The extension of the temporal bubble for more than 7 years leads to the progressive increase of the bias magnitude, which we attribute to the impact of the general deoxygenation. Based on these calculations, the 5-year threshold was selected as the maximum time separation between collocated profiles. For this threshold value, the number of collocated pairs below 1000m depth is about 10000 (**Fig. 16b**). A step-wise decrease of the number of collocated pairs below 950 m is explained by a significant part of reference profiles being limited to the upper 1000-meter layer. These calculations suggest that about 1000 collocated pairs are required for stable offset estimates.
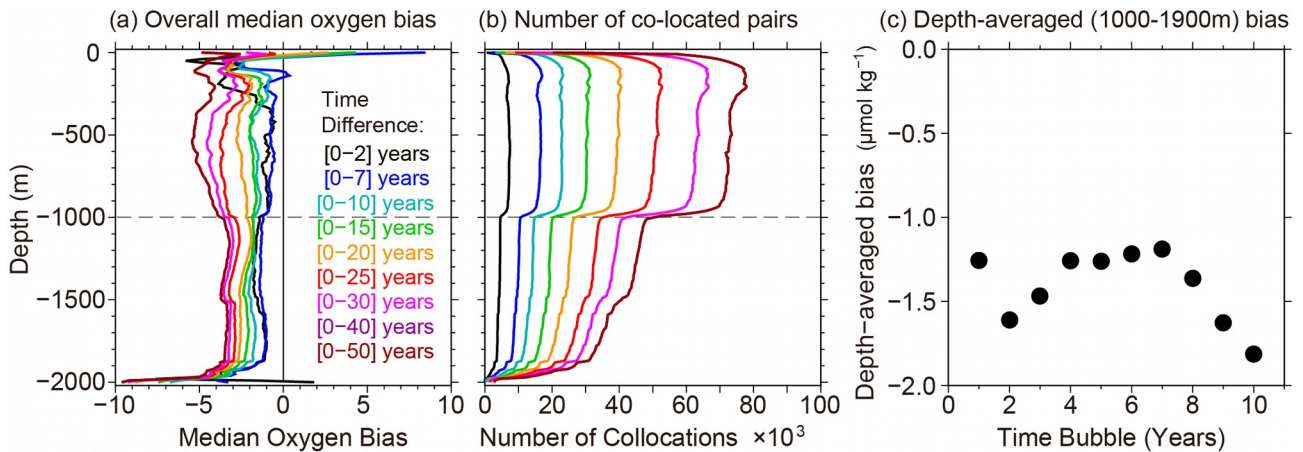
Figure 16. a) Overall median oxygen bias versus the size of the temporal collocation bubble; b) number of collocated pairs for different choices of collocation bubbles; c) depth-averaged (1000-1900m) bias versus time bubble size.

The number of Argo profiles having collocations with discrete ship-based Winkler profiles is shown in Table 1. No collocated Winkler profiles are found for the Argo profiles from the two Korean DACs. Profiles from these DACs are restricted within a relatively small area east of the Korean peninsula. The four largest contributors of Argo data (AOML, Coriolis, JMA, and CSIRO) comprise up to 90% of all Argo profiles having collocations with reference profiles.

6.2 Overall bias characteristics

The normalized frequency histograms (**Fig. 17**) characterize the spread of individual bias estimates around the distribution mode. These histograms are based on all Argo profiles having collocations with reference Winkler data. In these histograms, for each depth bin, the number of values in each bias bin is normalized by the number for the most populated bias bin at each depth level to account for the decrease of data with depth. The histograms are shown for raw (unadjusted) (Fig. 17a) and adjusted Argo profiles (Fig. 17b). The adjustment procedures applied at different DACs reduce the spread of the individual bias estimates and the skewness of the bias distribution, with the overall median bias of 10-12 µmol kg^{-1} for unadjusted data and 1-2 µmol kg^{-1} for adjusted data. As suggested by the bias distribution with depth, we estimate residual bias using the collocated data below 1000 m depth, where the bias spread reduces significantly compared to the upper part of the water column.
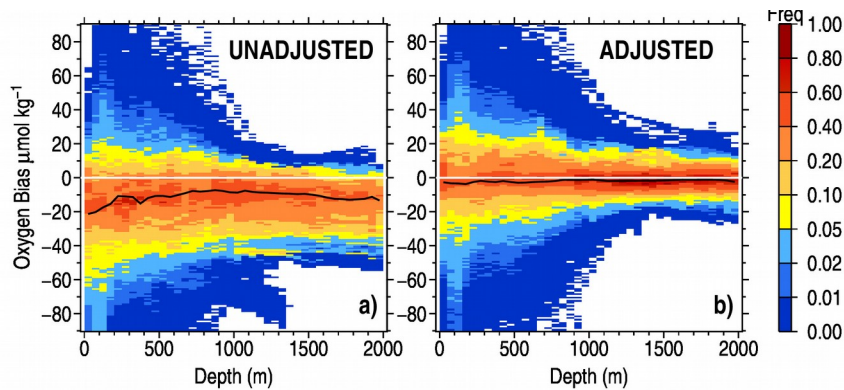
Fig.17. **Normalized histograms of the unadjusted (a) and adjusted (b) Argo oxygen bias versus collocated Winkler profiles. The black lines show the median bias value.**

6.3 Residual Oxygen Biases for Argo profiles from distinct DACs

According to the Argo Quality Control Manual (Thierry et al., 2021), several adjustment procedures can be applied to unadjusted data (adjustment to climatology, nearby Winkler samples, or in-air data). The adjustment results may depend on many factors, such as the subjective decision of the operator in a DAC, the use of a specific software, the availability of the respective reference data, and other factors. If a climatology is used as a reference, the Argo oxygen values will be adjusted to the median year of a climatology, which can differ by several decades from the year of an Argo profile. In such cases, the long-term deoxygenation trend of the world ocean might impact the results of the adjustment procedure.

Changes in oxygen sensors over time may cause respective changes in diagnosed biases. **Figure 18** shows the yearly number of observed profiles of AOML-processed Argo floats equipped with different models of optode sensors. Since the beginning of the 2000s, several different models of optodes have been implemented in BGC Argo floats, with the most widespread sensors being AANDERAA 3830, implemented between 2004 and 2018, and the following model AANDERAA 4330. Since about 2013, the majority of Argo floats from the two largest AOML and Coriolis datasets have been equipped with this sensor. The AANDERAA 4330 sensor prevails between 2012 and 2017 for JMA data and after 2020 for CSIRO data.
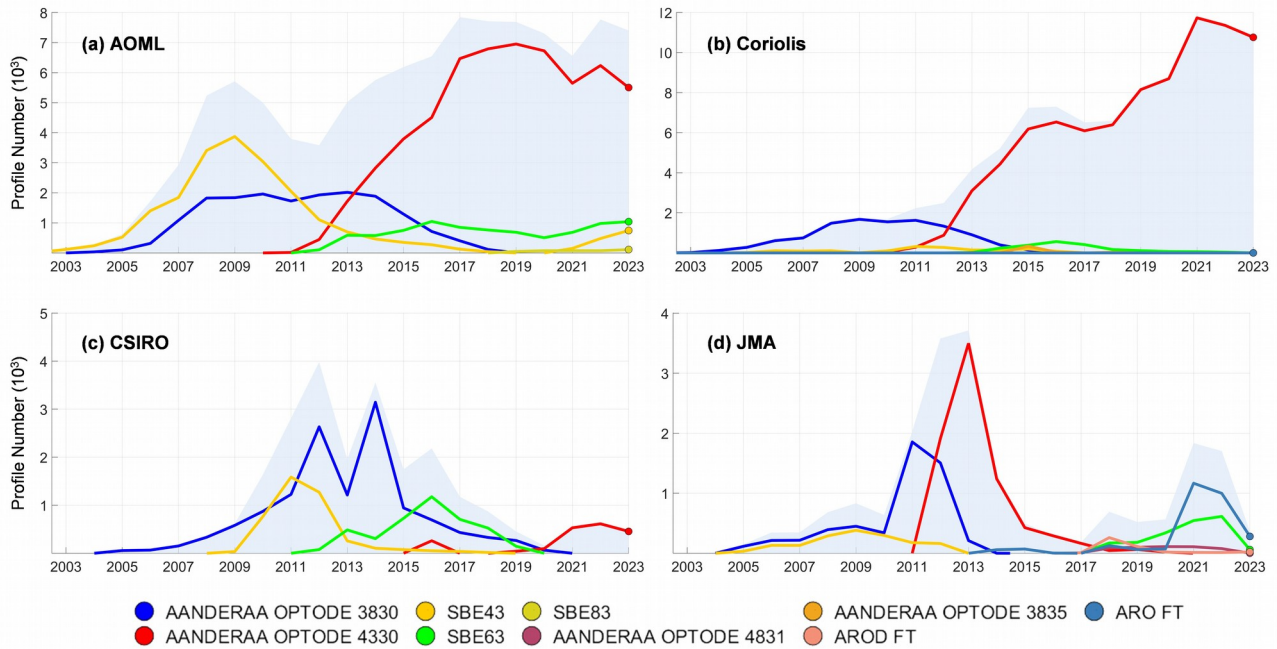
Figure 18. Annual numbers of BGC Argo profiles equipped with different types of optode oxygen sensors (coloured lines). Light-blue shading corresponds to the total number of profiles: (a) AOLM, (b) Coriolis, (c) CSIRO, and (d) JMA.

517   We calculated the residual oxygen bias for each depth level as the mean offset between Argo and Winkler oxygen

518 data over all collocated pairs for each DAC separately (**Fig. 19**). The offsets for the two Korean DACs cannot be

519 estimated due to the lack of the collocated Winkler profiles. The number of available collocations with reference

520 Winkler profiles varies by the order of magnitude for different DACs. Since reference bottle data often cover only part

521 of the upper 2000-meter layer, the number of collocated pairs also changes over depth, with the main step-wise decrease

522 seen around 1000 m. However, our calculations suggest that changes in the number of collocated pairs over depth do

523 not significantly impact the diagnosed bias. Except for CSIRO and BODC Argo profiles, DAC-adjusted overall median

524 residual bias is negative, ranging between -0.66 to -3.72 µmol kg^{-1}. The residual positive bias for CSIRO and BODC

525 profiles is within the range of 0.40-0.76 µmol kg^{-1} (we note that the BODC bias estimate is for the layer 100-1000m).

526 INCOIS profiles are characterized by the change from negative to positive bias below 1700 m.

527   For the two largest datasets (e.g., AOML and CORIOLIS) and the MEODS dataset, bias profiles exhibit a

528 characteristic hook below about 1900-1950 meters. Such hooks on Argo oxygen profiles were found by Thallander et

529 al., (2018). The hook can reflect the adjustment of the oxygen sensor at the beginning of the float ascending.

530   To investigate a possible bias change over time due to the change in the instrumentation (**see Fig. 18**), we

531 calculated depth-averaged biases (1000-1900m layer) for each collocation pair. Mean depth-averaged biases within

532 2°×4° latitude-longitude boxes are shown in **Fig. 20**, along with the bias histograms for two time periods: 2004-2013

533 and 2014-2023. The choice of these two periods approximately corresponds to the instrumentation change around 2013

534 (**Fig.18**). During the first period, the foil-batch calibrated optodes were used predominantly. Bittig et al., (2018) note

535 that differences between batch calibration and individual optode can exist. We find an indication of the instrumentation

536 shift only for the AOML dataset (**Fig. 20f**) and CSIRO (**Fig. 20p**) reflected in the shift of histograms to lower bias

537 values from 2004-2013 (-3.54 µmol kg^{-1}) to 2014-2023 (-0.25 µmol kg^{-1}). However, the second largest Coriolis dataset

does not show a significant difference between these two time periods (**Fig. 20i**), what could reflect differences in the adjustment procedures implemented by AOML and Coriolis DACs.
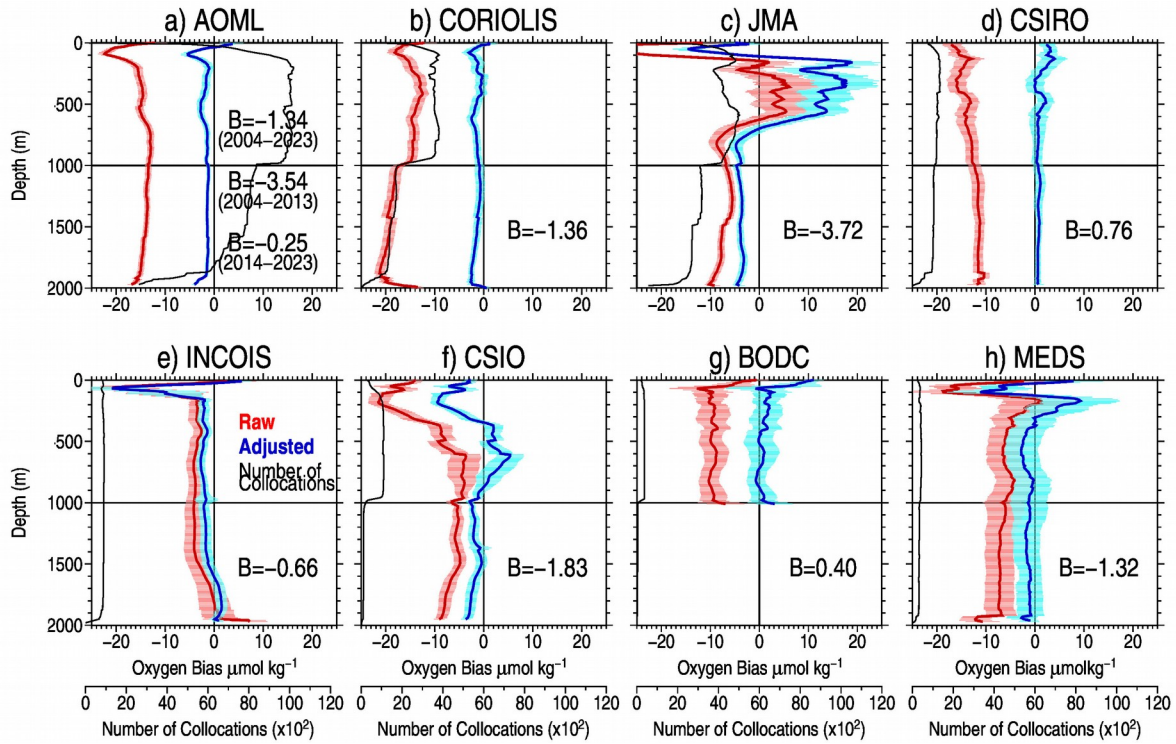
Figure 19. Overall mean Argo oxygen offsets vs Winkler profiles for distinct DACs: a) AOML, b) Coriolis, c) JMA, d) CSIRO, e) INCOIS, f) CSIO, g) BODC, h) MEDS. Offset profiles for unadjusted and adjusted data are shown in red and blue, respectively. Standard error bars (light shading) are calculated using the number of distinct floats at each level as the number of degrees of freedom. Blue numbers show the depth-averaged residual offsets (µmol kg^{-1}) within the layer 1000-1900m (for the BODC data, the depth-averaged offset is for the layer 100-1000m). Black thin lines show the number of collocated pairs at depth levels.

In addition to the overall biases described above, we calculated biases for distinct Argo floats (**Fig. 21**) using raw not-adjusted profiles and profiles with oxygen adjustments applied by the respective DACs. The floats are identified using their identification numbers. The number of collocations with Winkler profiles differs significantly among the floats. For the assessment of individual biases, we selected floats which have at least ten collocations with reference data (a total of 1020 floats). We found that adjustments applied to original raw oxygen profiles led to the bias reduction for 987 floats (96.9%), with only 33 floats (3.1%) showing a larger absolute bias than the unadjusted data. However, for the majority of these cases, the increase of the absolute bias value after adjustment does not exceed several µmol kg^{-1} and is well within the uncertainty of bias estimation for individual floats.

558
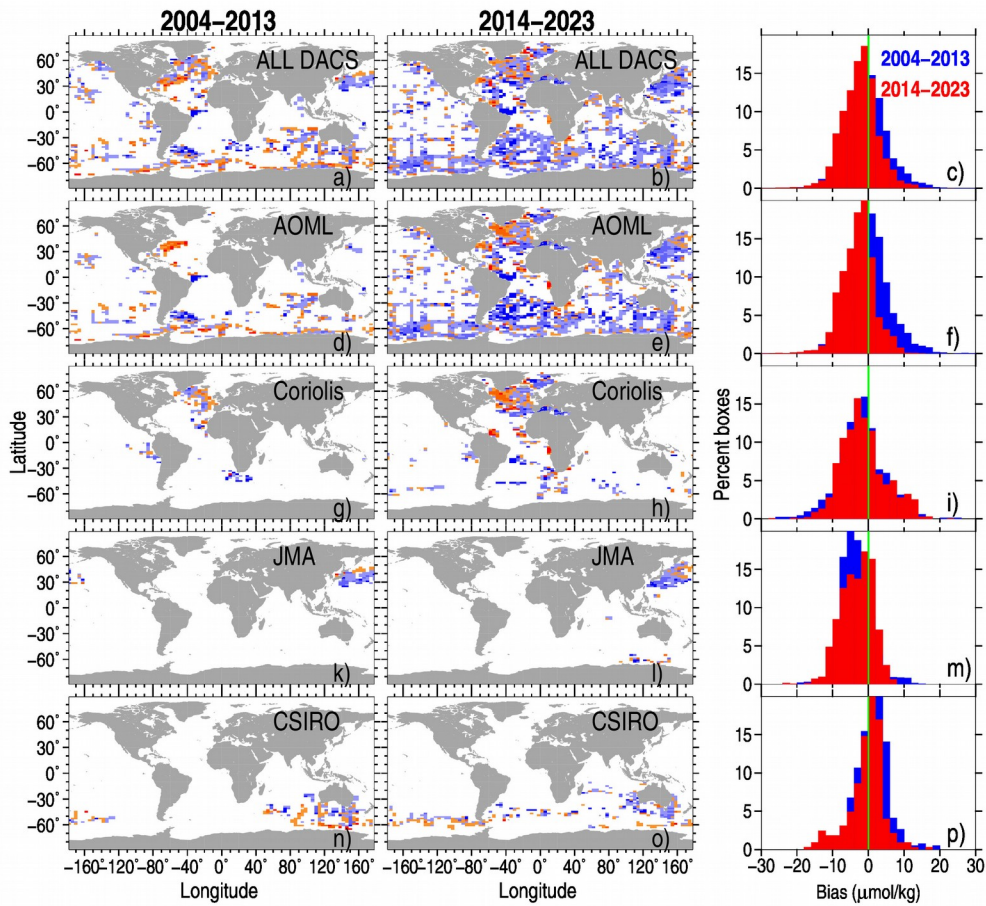
Figure 20. Mean oxygen bias for the layer 1000-1900m in 2°×4° boxes and histograms for the box-averaged biases for the entire Argo dataset: a) years 2004-2013; b) years 2014-2023; c) histograms of box-averaged biases for two time periods; d-f) same but for AOML data; g-i) same for Coriolis data; k-m) same for JMA data; n-p) same for JMA data; p-r) same for CSIRO data.

563
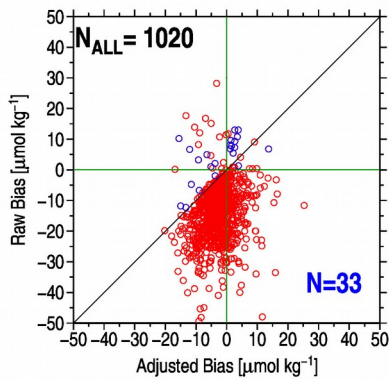
Figure 21. Oxygen bias for raw data versus bias for DAC-adjusted data for 1053 distinct Argo floats. For each Argo float the bias is calculated as the mean value within the layer 1000-1900m over all oxygen profiles having collocations with reference data. Blue circles correspond to the cases where the float bias magnitude for adjusted data exceeds that for the raw data.

565

7 Residual Oxygen Biases for CTD oxygen sensors

We conducted similar bias calculations for the CTD oxygen profiles, mostly obtained by electrochemical sensors. Only CTD data which passed all quality-controlled checks were used for the bias estimation. Unlike Argo profiles, the CTD oxygen sensor data are typically adjusted on the simultaneously collected bottle samples analyzed in the ship laboratory using the Winkler method (Thaillandier et al., 2018).

For 0-1900 m, we find an overall CTD oxygen offset of about 0.25 µmol kg^{-1} (median) relative to the Winkler data over the 1960-2022 period, which is much smaller than Argo oxygen biases ranging from -3.72 (JMA) to 0.76 µmol kg^{-1} (CSIRO) (**see Fig.19**). Similar to Argo data the offset distribution above 1000 m level (**Fig. 22e**) exhibits stronger spread than that below 1000 m. The median offset for the layer 1000-2000 m is 0.25 µmol kg^{-1}. Grégoire et al. (2021) indicated that "*the uncertainty associated with the last generation of O$_2$ sensors that uses the best calibration and calculation methods amounts, in the best case at ~2 µmol kg^{-1}*". Therefore, the overall median offset of 0.25 µmol kg^{-1} identified by this study is well within the expected uncertainty of the CTD sensors. Besides, there is no spatial uniform pattern for the CTD offsets (**Fig. 22d**), implying that this offset might not be systematic. Further investigation of the offsets for different cruises (figure not shown) indicates that the offset varies cruise by cruise and year by year. Therefore, in this study, we decided not to adjust the CTD data before the offset can be further confirmed after a cruise-by-cruise investigation and underlying reasons for the bias can be understood.
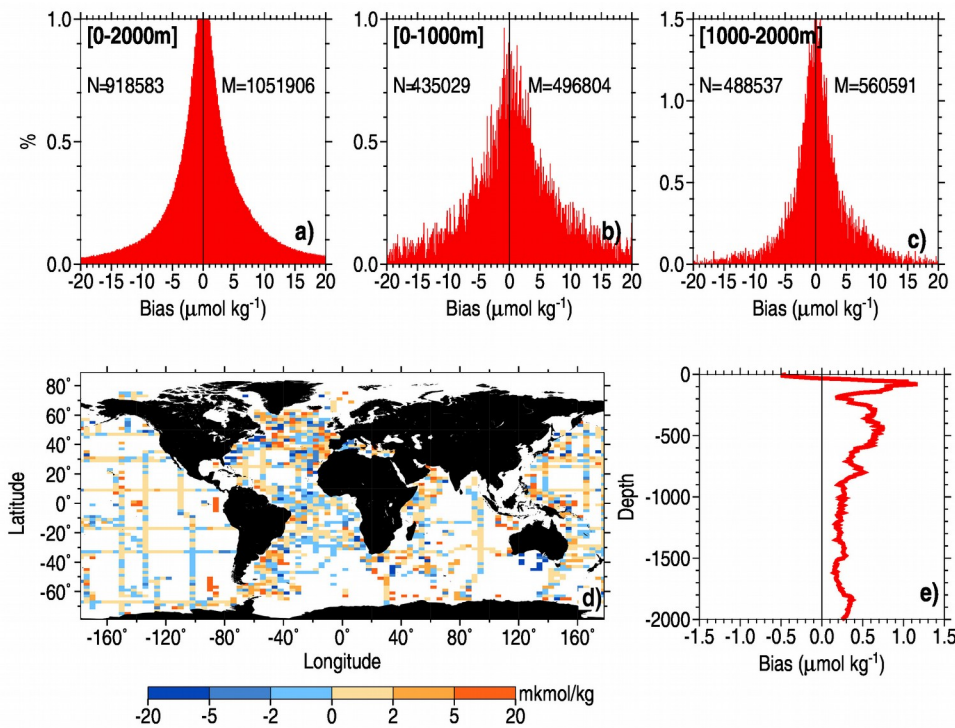
Figure 22. Statistics of the CTD oxygen bias relative to co-located Winkler data. Histograms of layer-averaged bias for 0-2000 m (a), 0-1000 m (b) and 1000-2000 m (c). Number of negative (N) and positive (M) bias values is shown respectively on the left and right side of each histogram. (d) median of depth-averaged offset (1000-2000m) in 2°×4° grid boxes; (e) overall median CTD oxygen offset as a function of depth.

8   Conclusion and Discussion

This study developed a new automated QC scheme for ocean oxygen profile data and applied it to the oxygen profiles from the WOD and the Argo float oxygen profiles provided by national DACs. The procedure consists of a suite of ten quality checks, which are based on local or global parameter thresholds. Some checks are conceptually similar to the quality checks used to validate the profiles in the World Ocean Database (Boyer et al., 2018) (for example, the global range test, and vertical gradient test) and in the Argo data acquisition centers (Thierry et al., 2021) (for example, spike, frozen profile tests), but we provide additional checks (for example, test for the number of local extrema and local climatological range test) which increase the ability of the QC procedure to better identify erroneous data. For instance, the procedure proves whether an oxygen value falls out of accepted ranges (defined by global or local ranges) or whether an oxygen profile exhibits a very untypical shape. The shape of the profile is characterized by the vertical oxygen gradient, the number and magnitude of local oxygen extrema, and the presence of spikes. The check is also done for the so-called "frozen" profiles occurring when the oxygen sensor stucks and reports the same values throughout the profile.

The QC procedure presented here is tailored for the quality assessment of the archived oxygen data obtained both by Winkler methods and sensors. Large ocean depositories like WOD often contain observed data which already undergone a certain degree of QC and adjustment. Therefore, our QC procedure differs from the real-time QC of dissolved oxygen observations by means of oxygen sensors as suggested in the frame of the Integrated Ocean Observing System (IOOS) in the quality control manual by Bushnell et al. (2015) (B2015 hereafter). Three quality tests which have been required or suggested in that manual can be applied only to the real time data: the application of the gap test needs the time stamp of each measurement, the application of the syntax test requires the full original data record, and the application of the neighbor test is possible only in the case when a nearby second sensor is installed on the device. Information needed for these tests is not kept in the WOD therefore these tests can not be applied to "static" archive data. Five other tests outlined in B2015 are conceptually similar to the tests applied by our QC procedure: location test, gross range test, climatology test (all three required by B2015), spike test and flat line test (both recommended by B2015). In a deviation from our QC procedure, thresholds for test variables according to B2015 should be chosen subjectively by operators in the data centers. We note that the metadata on decisions made operators are usually missing in the data archives.

The novelty of the proposed quality scheme is that the threshold choice is based on the respective statistics of test variables, and the Gaussian distribution is not assumed for the important local climatological range checks for oxygen and for oxygen vertical gradient. The QC procedure presented in this study was benchmarked against several hydrographic datasets known for their outstanding measurement quality, with WOCE experiment data collection being the largest and best documented. Analysis of the outliers and their distribution among distinct hydrographic sections suggests the ability of the procedure to flag outliers but retain the overwhelming majority of good data. The accompanying diagnostic tool provides the overview of outlier scores and permits tuning of thresholds when new benchmark quality-controlled datasets become available. Finally, we note that the transparent choice of test threshold values on the basis of the underlying statistics and the subsequent analysis of outliers for each quality check permits further tuning of the quality control procedure in order to increase the percentage of true outliers and to decrease the percentage of falsely identified outliers.

623   Further, we estimated possible residual oxygen biases in the delayed-mode adjusted Argo oxygen profiles. The bias

624   estimates are based on the collocated Argo and discrete water sample ship-based profiles. The latter represents reference

625   measurements as the bottle samples are analyzed by means of the Winkler chemical method. The size of the collocation

626   bubble (e.g., the maximum distance between two profiles and the maximum time difference) was set at 100 km and 5

627   years, respectively, after several experiments with different bubble sizes. Residual biases relative to the Winkler

628   reference data are represented by the difference at an isobaric level between the Argo sensor oxygen value and the

629   Winkler oxygen, with the overall residual bias at each level being defined by the average overall individual differences.

630   To reduce the impact of time- and spatial variability, the final bias assessment is done for the layer 1000-1900m, which

631   is typically located below the main thermocline.

632   Our calculations find a negative residual oxygen bias in the range -0.66 to -3.72 $\mu mol\ kg^{-1}$ for all individual DAC

633   datasets except CSIRO and MEDS. The residual positive bias for CSIRO and BODC profiles is within the range of

634   0.40-0.76 $\mu mol\ kg^{-1}$. This bias is crucial to accurately identify the deoxygenation trend, as current assessments suggest

635   an upper 1000 m O_2 content decrease of 0.2–1.2 $\mu mol\ kg^{-1}\ dec^{-1}$ during 1970–2010 (Gulev et al. 2023). Out calculations

636   suggest that at least 1000 collocation pairs are needed for the stable residual bias estimation. This number of

637   collocations is available only for AOML, Coriolis, JMA, CSIRO, and INCOIS datasets. Further, we found a change in

638   the diagnosed residual oxygen bias around 2014 for the largest AOML dataset, possibly related to the instrumentation

639   change, when the AANDERAA optode A4330 became the primary sensor type used on Argo floats. However, this

640   change in the residual bias could not be diagnosed for the second-largest Coriolis dataset. Analysis of the residual bias

641   for 1053 Argo floats having at least ten profiles with collocations confirmed bias reduction for 97% of the floats

642   (compared to the unadjusted data) due to the adjustments conducted by DACs.

643   Diagnosed residual biases for the quality-controlled CTD oxygen sensor profiles revealed a good agreement

644   between the CTD and Winkler reference data, with a small median bias of 0.25 $\mu mol\ kg^{-1}$ within the layer below 1000

645   m. Because of a relatively small bias value, which is well within the uncertainty of the CTD sensors and due to a non-

646   uniform spatial CTD bias pattern, the diagnosed overall bias is not considered to be a common and robust feature, and

647   no adjustment of CTD data is performed in this study. Our preliminary investigation also indicates that the CTD offset

648   varies cruise-by-cruise, probably associated with the differences in the calibration or re-calibration (or post-processing).

649   Therefore, the follow-on work should include investigating the offsets on a cruise-by-cruise basis and providing an

650   understanding of the causes of bias. Only after these examinations are done can an adjustment on CTD be physically

651   tenable.

652   This study also has some limitations and caveats: (1) Although systematical errors have been identified for Argo

653   oxygen data, the cause of the biases is still poorly known and requires further work. The differences between the DAC

654   centers are also mysterious, and we suspect that the non-standard adjustment procedure developed by different National

655   Argo Data Centers and the difference in sensors on Argo floats used in different countries might be responsible for the

656   differences in diagnosed biases, which needs further confirmation. (2) Because the sources of biases are poorly known,

657   the correction proposed in our study is largely empirical and only applies to the Argo data used in this study. If the

658   Global Argo Data Center updates quality control and adjustment procedures, our bias corrections also require an update.

659   (3) The QC procedure is designed to detect and flag the outliers. However, there are also risks of removing the "real

660   extremes" in the ocean, especially under rapid climate change, as ocean extreme events are expected to become more

661   frequent. One possible way to partly resolve this problem is imposing a trend in the local climatological range,

662   accounting for the time-variation of the local oxygen distributions with climate change, which would help to reduce the

false flag percentage of the real extreme data in the ocean. This requires further work when the local oxygen trends become clearer. (4) The Winkler data are used in this study as a reference. However, it is also possible that the Winkler data are not taken to the same standard, thus posing inconsistency within the Winkler dataset, especially for the data taken by different countries and time periods. Investigating the offsets on a cruise-by-cruise basis is also recommended in the future, as for CTD data.

In summary, this study proposed a new quality control approach and bias assessment for the CTD, bottle, and Argo oxygen data and investigated the consistency between these three primary instrumentation types. Our investigations ensured the consistency between the three datatypes and provided a solid basis for merging them into a single, integrated, and homogeneous oxygen database. Therefore, the database obtained in this study supports the next-step assessment and understanding of the change in ocean oxygen levels.

7   Data availability

The quality control procedure described above was applied to the OSD and CTD oxygen profiles between 1920 and 2023 from the World Ocean Database and to the oxygen profiles from the BGC Argo floats. The resulting dataset comprises observed level data with quality flags and data interpolated on 10-meter levels. The data are in NetCDF format and also include the metadata information. The complete dataset (Gouretski et al., 2023) can be found at http://dx.doi.org/10.12157/IOCAS.20231208.001.

Author contributions.

LC and VG – conceptualization, supervision, methodology; VG – software, formal analysis, data validation, visualization, and writing (original draft preparation, final version, and editing); JD, XX, FC – methodology, data curation; LC – writing, analysis, methodology, funding acquisition.

Competing interests. The contact author has declared that none of the authors has any competing interests.

Acknowledgements. We are thankful to the colleagues from the National Centers for Environmental Information (NCEI) and the Argo Global Assembly Center (GDAC) for providing access to the data used in this study (specific Argo DACs are noted in the text). We also thank two anonymous reviewers for their detailed and constructive comments. The Argo data were collected and made freely available by the International Argo Program and the national programs that contribute to it (ARGO, 2000). The Argo Program is part of the Global Ocean Observing System.

Financial support. This study was supported by the Strategic Priority Research Program of the Chinese Academy of Sciences [grant number XDB42040402], the National Natural Science Foundation of China [grant numbers 42122046 and 42076202], and the Youth Innovation Promotion Association, CAS [grant number 2020-077]. The author also acknowledges the support from the new Cornerstone Science Foundation through the XPLORER PRIZE, Youth Innovation Promotion Association, Chinese Academy of Sciences.

700

References

Adil, I. H. and Irshad, A. R.:A modified approach for detection of outliers, Pak. J. Stat. Oper. Res., XI, 1, 91-102.

Argo (2000). Argo float data and metadata from Global Data Assembly Centre (Argo GDAC). EANOE. https://doi.org/10.17882/42182

Bittig, H. C., Maurer, T.L., Plant, J. N., Schmechtig, C., Wong,A. P. S. , Claustre,H., Trull, T. W. , Udaya Bhaskar, T. V. ., Boss, E., Dall'Olmo, G., Organelli, E., Poteau, A., Johnson, K. S., Hanstein, Leymarie,C., E., Le Reste, S., Riser, S. C., Rupan, A., Taillandier, V., Thierry, V. and Xing, X. : A BGC-Argo Guide: Planning, Deployment, Data Handling and Usage, Front. Mar. Sci., 6:502, doi: 10.3389/fmars.2019.00502, 2018.

Baranova, O. K., Seidov, D., and Reagan, J. R.: World Ocean Atlas 2018, Volume 3: Dissolved Oxygen, Apparent Oxygen Utilization, and Oxygen Saturation. A. Mishonov Technical Ed.; NOAA Atlas NESDIS 83, 38pp, 2018.

Breitburg, D. et al. Declining oxygen in the global ocean and coastal waters. Science 359, eaam7240 (2018).

Bittig, H. C., and Körtzinger, A. (2015). Tackling oxygen optode drift: Near-surface and in-air oxygen optode measurements on a float provide an accurate in situ reference. *J. Atmos. Ocean. Technol.* 32, 1536–1543. doi: 10.1175/JTECH-D- 14- 00162.1

Boyer, T. P., Baranova, O.K., Coleman, C., Garcia, H. E. , Grodsky, A., Locarnini, R. A.,Mishonov, A. V., Paver, C. R.,Reagan, J. R. , Seidov, D., Smolyar, I. V., Weathers, K., Zweng, M.M.: World Ocean Database 2018, A. V. Mishonov, Technical Editor, NOAA Atlas NESDIS 87, 2018.

Bushnell, M., R. Toll., and H. Worthington: Manual for real-time quality control of dissolved oxygen observations : a guide to quality control and quality assurance for dissolved oxygen observations in coastal oceans, Integrated Ocean Observing System (U.S.), DOI : http://doi.org/10.7289/V5ZW1J4J, 2015.

Carpenter, J.H. :The accuracy of the Winkler method for dissolved oxygen analysis, Limnology and Oceanography, 10, 1, p. 135-140. https://doi.org/10.3419/lo.1965.10.1.0135, 1965.

Cheng, L. J., Zhu, J., Cowley, R., Boyer, T. and Wijffels, S.: Time, probe type and temperature variable bias corrections to historical expendable bathyther-mograph observations, J. Atmos. Ocean. Technol.,31, 1793–1825, doi:10.1175/JTECH-D-13-00197.1, 2014.

Clark, L. C.: Cellophane/Platinum electrode for blood PO2, J. Appl. Physiology, 6, 189, 1953.

Claustre, H., Johnson, K. S., and Takeshita, Y.: Observing the global ocean with biogeochemical-Argo, Annual Review of Marine Science, 12, 23–48, 2020.

Coppola, L., Salvetat, F., Delauney, L., Machoczek, D., Larstensen, J., Sparnocchia, S.,Thierry, V., Hydes, D., Haller, M.,Nair, R., Lefevre, D.: White paper on dissolved oxygen measurements: scientific needs and sensors accuracy, 22 pages, 2013.

Cowley, R., Killick, R. E., Boyer, T., Gouretski, V., Reseghetti, F., Kizu, S., Palmer, M. D., Cheng, L., Storto, A., Le Menn, M., Simoncelli, S., Macdonald, A. M., and Domingues, C. M.: International Quality-Controlled Ocean Database (IQuOD) v0.1: The Temperature Uncertainty Specification, Front. Mar. Sci. 8:689695. doi: 10.3389/fmars.2021.6896, 2021

Craig, H.: The GEOSECS program: 1972-1973: Earth Planetary Science Letters, v 23, p 63–64., 1974

Falck, E. and Olsen, A.: Nordic Seas dissolved oxygen data in CARINA, Earth Syst. Sci. Data, 2, 123–131, https://doi.org/10.5194/essd-2-123-2010, 2010.

Baranova, O. K., Seidov, D., and Reagan, J. R.: World Ocean Atlas 2018, Volume 3: Dissolved Oxygen, Apparent Oxygen Utilization, and Oxygen Saturation. A. Mishonov Technical Ed.; NOAA Atlas NESDIS 83, 38pp, 2018.

Deutsch, C., Brix, H., Ito, T., Frenzel, H. & Thomson, L. Climate-forced variability of ocean hypoxia. *Science* **333**, 336–339 (2011).

Golterman, H. L. The Winkler Determination. In: Gnaiger, E., Forstner, H. (eds) Polarographic Oxygen ensors. Springer, Berlin, Heidelberg. https://doi.org/10.1007/978-3-642-81863-9_31, pp.346-351, 1983.

745 Garcia H. E., Z. Wang, C. Bouchard, S.L. Cross, C.R. Paver, J.R. Reagan, T.P. Boyer, R.A. Locarnini, A.V. Mishonov,
746   O.K. Baranova, D. Seidov, and D. Dukhovskoy (2024). World Ocean Atlas 2023, Volume 3: Dissolved Oxygen,
747   Apparent Oxygen Utilization, Dissolved Oxygen Saturation, and 30-year Climate Normal. A. Mishonov Technical
748   Editor. *NOAA Atlas NESDIS 91,* 100 pp. https://doi.org/10.25923/rb67-ns53

749 Good., S., Mills, B., Boyer T., Bringas, F., Castelão, G., Cowley, R., Goni, G., Gouretski, V. and Domingues, C. M.:
750   Benchmarking of automatic quality control checks for ocean temperature profiles and recommendations for
751   optimal sets, Front. Mar. Sci., DOI 10.3389/fmars.2022.1075510, 2022.

752 Gulev, S. *et al.* Changing state of the climate system. In *climate change 2021: The physical science basis. Contribution*
753   *of working group I to the sixth assessment report of the intergovernmental panel on climate change* (eds Masson-
754   Delmotte, V. et al.). (Cambridge Univ. Press, 2021).

755 Gruber, N., Doney, S. C., Emerson, S. R., Gilbert, D., Kobayashi, T., Körtzinger, A., et al. (2010). "Adding oxygen to
756   argo: Developing a global in situ observatory for ocean deoxygenation and biogeochemistry," in *Proceedings of*
757   *Ocean Obs '09: Sustained Ocean Observations and Information for Society*, eds J. Hall, D. E. Harrison, and D.
758   Stammer (New Zealand: ESA Publication), 12. doi: 10.5270/ OceanObs09.cwp.39

759 Garcia H. E., Z. Wang, C. Bouchard, S.L. Cross, C.R. Paver, J.R. Reagan, T.P. Boyer, R.A. Locarnini, A.V. Mishonov,
760   O.K. Baranova, D. Seidov, and D. Dukhovskoy (2024). World Ocean Atlas 2023, Volume 3: Dissolved Oxygen,
761   Apparent Oxygen Utilization, Dissolved Oxygen Saturation, and 30-year Climate Normal. A. Mishonov Technical
762   Editor. *NOAA Atlas NESDIS 91,* 100 pp. https://doi.org/10.25923/rb67-ns53

763 Gruber, N. Warming up, turning sour, losing breath: ocean biogeochemistry under global change. Phil. Trans. R. Soc. A
764   369, 1980–1996 (2011).

765 Gouretski, V., Cheng, L., Du, J., Xing, X., Chai, F.: A quality-controlled and bias-adjusted global ocean oxygen profile
766   dataset, Marine Science Data Center of the Chinese Academy of Sciences,
767   http://dx.doi.org/10.12157/IOCAS.20231208.001

768 Gouretski, V.: World Ocean Circulation Experiment – Argo Global Hydrographic Climatology, Ocean Sci., 14, 1127-
769   1146, https://doi.org/10.5194/os-14-1127-2018, 2018.

770 Gouretski, V. and Reseghetti, F.: On depth and temperature biases in bathythermograph data: development of a new
771   correction scheme based on analysis of a global database, Deep-Sea Res., I, 57, 812-833, 2010.

772 Gouretski, V. V., and Jancke, K.:Systematic errors as the cause for an apparent deep water property variability: global
773   analysis of the WOCE and historical hydrographic data., Prog. Oceanogr., 48, 4, 337-402, 2000.

774 Gregoire, M. et al.: A Global Ocean Oxygen Database and Atlas for Assessing and Predicting Deoxygenation and Ocean
775   Health in the Open and Coastal Ocean, Front. Mar. Sci., 8, 1-29,https://doi.org/10.3389/fmars.2021.724913 , 2021.

776 Helm, K. P., Bindoff, N. L. & Church, J. A. Observed decreases in oxygen content of the global ocean. *Geophys. Res.*
777   *Lett.* **38**, L23602 (2011).

778 Hood, E.M., Sabine, C.L., and M. Sloyan, B.M., eds.:The GO-SHIP Repeat Hydrography Manual: A Collection of
779   Expert Reports and Guidelines, IPCC Report Number 14, ICPO Publication Series Number 134, 2010.

780 Hubert, M. and Vandervieren, E.: An Adjusted boxplot for skewed distributions, Comput. Stat. Data Anal., 52, 5186–
781   5201, 2008.

782 Keeling, R.F., Koetzinger, A., and Gruber, N.: Ocean Deoxygenation in a Warming world, Annu. Rev. Mar. Sci., 2, 199-
783   229. doi:10.1146/annurev.marine.010908.163855, 2010.

784 Koertzinger, A., Schimanski, J., and Send, U.: High quality oxygen measurements from profiling floats: A promising
785   new technique, J. Atmos. Ocean. Technol., 22, 302-308, 2005

786 Ito, T., Minobe, A., Long, M. C. & Deutsch, C. Upper ocean O_2 trends: 1958–2015. *Geophys. Res. Lett.* **44**, 4214–4223
787   (2017).

788 Langdon, C.: Determination of Dissolved Oxygen in Seaweater By Winkler Titration using Amperometric Technique,
789   The GO-SHIP Repeat Hydrography Manual: A Collection of Expert Reports and Guidelines, Version 1, (eds Hood,

E.M., C.L. Sabine, and B.M. Sloyan), 18pp.. (IOCCP Report Number 14; ICPO Publication Series Number 134), DOI: https://doi.org/10.25607/OBP-1350, 2010.

Larqué, L., Maamaatuaiahutapu, K., Garçon, V.: On the intermediate and deep water flows in the South Atlantic Ocean. Journal of Geophysical Research, 102,C6, https://doi.org/10.1029/97JC00629, 1997.

Long, M. C., Deutsch, C. & Ito, T. Finding forced trends in oceanic oxygen. *Global Biogeochem. Cycles* **30**, 381–397 (2016).

Levin, L. A. Manifestation, drivers, and emergence of open ocean deoxygenation. *Annu. Rev. Mar. Sci* **10**, 229–260 (2018).

Johnson, K. S., Plant, J., Coletti, L., Jannasch, H., Sakamoto, C., Riser, S., et al. (2017). Biogeochemical sensor performance in the SOCCOM profiling float array. *J. Geophys. Res. Oceans* 122, 6416–6436. doi: 10.1002/2017JC012838

Marks, R.: Dissolved oxygen supersaturation and its impact on bubble formation in the southern Baltic Sea, Hydrol. Res., 39,3, 229-236, 2008.Monhor, D. and Takemoto, S.: Understanding the concept of outlier and its relevance to the assessment ofdata quality: Probabilistic background theory, Earth Planets Space, 57, 1009–1018, 2005.

Oschlies, A. et al. Patterns of deoxygenation - sensitivity to natural and anthropogenic drivers. *Phil. Trans. Roy. Soc. A* **375**, 20160325 (2017).

Praetorius, S. K. et al. North Pacific deglacial hypoxic events linked to abrupt ocean warming. *Nature* **527**, 362–366 (2015).

Pitcher, G. C., Aguirre, A., Breitburg, D., Cardich, J., Carstensen, J., Conley, D. J., et al. (2021). System controls of coastal and open ocean oxygen depletion. Prog. Oceanogr. 197:102613. doi: 10.1016/j.pocean.2021.102613

Roemmich, D., Alford, M. H., Claustre, H., Johnson, K., King, B., Moum, J., et al. (2019). On the future of Argo: An enhanced global array of physical and biogeochemical sensing floats. Front. Mar. Sci. 6:439. . doi: 10.3389/fmars.2019. 00439

Sarachik, E.S.: CLIVAR: A Study of Climate Variability and Predictability: Science Plan. World Climate Research rogramme Report 89, WMO Technical Document No 690. 157 pp, 1995.

Stramma, L., Oschlies, A., and Schmidtko, S.: Mismatch between observed and modeled trends in dissolved upper-ocean oxygen over the last 50 yr, Biogeosciences, 9, 4045–4057, https://doi.org/10.5194/bg-9-4045-2012, 2012.

Schmidtko, S., Stramma, L. & Visbeck, M. Decline in global oceanic oxygen content during the past five decades. *Nature* **542**, 335–339 (2017).

Schmidtko, S., Stramma, L. & Visbeck, M. Decline in global oceanic oxygen content during the past five decades. *Nature* **542**, 335–339 (2017).

Taillander, V., Wagener, T., D'Ortenzio, F., Mayot, N., Legoff, Ras, H. J., Coppola, L., De Fommervault, O. P., Schmechtig, C., Diamond, E., Bittig, H., Lefevre, D., Leymarie, E., Poteau, A., and Prieur A.: Hydrography and biogeochemistry dedicated to the Mediterranean BGC-Argo network during a cruise with RV Tethys 2 in May 2015, Earth Syst. Sci. Data, 10, 627-641, 2018, https://doi.org/10.5194/essd-10-627-2018, 2018.

Takeshita, Y., Martz, O. P., Johnson, K. S., Plant, J. N., Gilbert, D., Riser, S. C., Neil, C., and Tilbrook, B.: A climatology-based quality control procedure for plotting float oxygen data, J. Geoph, Res: Oceans, 118, 1-11, doi:10.1002/jgr.20399, 2013.

Tan, Z., Cheng, L., Gouretski, V., Zhang, B., Wang, Y., Li, F., Liu, Z., Zhu, J.: A new automatic quality control system for ocean profile observations and impact on ocean warming estimate, Deep-Sea Res. Part I: Oceanographic Research Papers, 194, https://doi.org/10.1016/j.dsr.2022.103961, 2023.

Tengberg, A., Hovdenes, J., Andersson, H. J., Brocandel, O., Diaz, R., Hebert, D., Arnerich, T., Huber, C ., Körtzinger, A., Khripounoff, A., Rey, F., Rönning, C., Schimanski, J., Sommer, S. and Stangelmayer, A. : (2006): Evaluation of a lifetime-based optode to measure oxygen in aquatic systems. Limnol. Oceanogr.: Methods, 4, 7-17, 2006.

835   Thierry, V., Bittig, H., and the Argo-BGC team: Argo quality control manual for dissolved oxygen concentration,
836   Version 2.1, Argo Data Management, doi: https://dx.doi.org/10.13155/46542, 2021.

837   Tukey, J. W. Exploratory Data Analysis, ed. Pierson, ISBN-10: 0201076160, 503 pp., 1977.

838   Uchida, H., Johnson, G. C., and McTaggart, K. E.: CTD Oxygen sensor calibration procedures. The Go-SHIP
839   Hydrography Manual: A Collection of Expert Reports and Guidelines. IOCCP Report No. 14, ICPO Publication
840   Series No. 134, Version 1, 17p., 2010.

841   WHPO: WOCE Operations Manual, Section 3.1.3: WHP operations and methods,WOCE report no. 69/91, WHPO 91-1.
842   80 pp., 1991.

843   Winkler, L.: Die Bestimmung des in Wasser gelosten Sauerstoffes. Berichte der Deutschen Chemischen Gesellschaft. 21
844   (2): 2843–2855. doi:10.1002/cber.188802102122, 1888.

845   Wunsch, C.: Towards the World Ocean Circulation Experiment and a bit of aftermath, Springer-Verlag, Jochum, M.,
846   Murtugudde, R., Phys. Oceanogr., 181-201, 2006.

847   Yang, J., Rahardja, S., and Fränti, P.: Outlier Detection: How to Threshold Outlier Scores?, AIIPCC '19: Proceedings
848   of the International Conference on Artificial Intelligence, Information Processing and Cloud Computing,
849   December 2019. Article No.: 37, p. 1–6 https://doi.org/10.1145/3371425.3371427, 2019.